Carbon cycle and climate feedbacks under CO_2 and non-CO_2 overshoot pathways

Irina Melnikova[1,2], Philippe Ciais[2], Katsumasa Tanaka[1,2], Hideo Shiogama[1], Kaoru Tachiiri[1,3], Tokuta Yokohata[1] and Olivier Boucher[4]

[1]Earth System Division, National Institute for Environmental Studies (NIES), Tsukuba, 305-8506, Japan,
[2]Laboratoire des Sciences du Climat et de l'Environnement (LSCE), IPSL, CEA/CNRS/UVSQ, Université Paris-Saclay, Gif-sur-Yvette, 91191, France
[3]Research Institute for Global Change, Japan Agency for Marine-Earth Science and Technology, Yokohama, 236-0001, Japan
[4]Institut Pierre-Simon Laplace, Sorbonne Université / CNRS, Paris, 75005, France

Correspondence to: Irina Melnikova (melnikova.irina@nies.go.jp)

Abstract. Reducing emissions of non-CO_2 greenhouse gases, such as methane and nitrous oxide, complements CO_2 mitigation in limiting global warming. However, estimating carbon-climate feedback for these gases remains fraught with uncertainties, especially under overshoot scenarios. This study investigates the impact of CO_2 and non-CO_2 gases with nearly equal levels of effective radiative forcing on the climate and carbon cycle, using the Earth System Model IPSL-CM6A-LR. We first present a method to recalibrate methane and nitrous oxide concentrations to align with published radiative forcings, ensuring accurate model performance. Next, we carry out a series of idealised ramp-up and ramp-down concentration-driven experiments and show that while the impacts of increasing and decreasing CO_2 and non-CO_2 gases on the surface climate are nearly equivalent (when their radiative forcing magnitudes are set to be the same), regional differences emerge. We further explore the carbon cycle feedbacks and demonstrate that they differ under CO_2 and non-CO_2 forcing. CO_2 forcing leads to both carbon-climate and carbon-concentration feedbacks, whereas non-CO_2 gases give rise to the carbon-climate feedback only. We introduce a framework, building on previous studies that addressed CO_2 forcing, to separate the carbon-climate feedback into a temperature term and a temperature–CO_2 cross term. Our findings reveal that these feedback terms are comparable in magnitude for the global ocean. This underscores the importance of considering both terms in carbon cycle feedback framework and climate change mitigation strategies.

Plain language summary. Mitigating non-CO_2 greenhouse gases, like methane and nitrous oxide, complements efforts to reduce CO_2 emissions in limiting global warming. In our study, we explore how reducing emissions of these gases compares to CO_2 mitigation using an Earth System Model. Both types of gases contribute to global warming, but their effects on climate vary by region. Additionally, we highlight that the carbon cycle responds differently depending on whether climate change is driven by CO_2 or non-CO_2 gases. This highlights the importance of considering both types of gases within carbon cycle analysis framework and climate change mitigation strategies.

1 Introduction

Increases in the atmospheric concentrations of carbon dioxide (CO_2), methane (CH_4), and nitrous oxide (N_2O), predominantly cause human-induced climate change since the preindustrial period. They contributed nearly 63%, 11% and 6%, respectively, to the total effective radiative forcing (ERF) over 1960–2019 period (Canadell et al., 2021). Anthropogenic CO_2 emissions are dominated by the combustion of fossil fuels (FF) and land-use change (LUC), CH_4 emissions by FF and the agricultural sector, and N_2O emissions by the use of nitrogen fertiliser and manure. CH_4 and N_2O have atmospheric lifetimes of 11.8 ± 1.8 years and 109 ± 10 years and 100-year global warming potentials (GWP100) of 27.9 and 273, respectively (Forster et al., 2021; Myhre et al., 2013).

Mitigation of non-CO_2 greenhouse gases (GHGs) is an essential strategy to limit global warming in the context of the Paris Agreement's temperature target (Abernethy et al., 2021; Jones et al., 2018; Rao and Riahi, 2006; de Richter et al., 2017; Tanaka et al., 2021). The reduction of CH_4 emissions can lead to a rapid decrease in the radiative forcing and may limit the peak warming (Mengis and Matthews, 2020; Montzka et al., 2011). To facilitate the achievement of the Paris Agreement temperature target, the Global Methane Pledge was adopted to reduce anthropogenic CH_4 emissions by 30% over the 2020–2030 period (CCAC, 2021). Several existing studies have confirmed the technical and socioeconomic capacities to reduce the global methane emissions and benefits for reducing atmospheric pollution (Höglund-Isaksson et al., 2020; Jackson et al., 2021; Malley et al., 2023; Nisbet et al., 2020). Atmospheric methane removal methods have also been discussed in some studies (Boucher and Folberth, 2010; Jackson et al., 2021; Mundra and Lockley, 2023) but they are still in their infancy.

Numerous studies have investigated the impacts of changes in the emissions / concentrations of CO_2 and non-CO_2 GHGs on the Earth System. The Precipitation Driver and Response Model Intercomparison Project (PDRMIP) focused on the role of different climate change drivers on the mean and extreme precipitation changes using a set of idealised perturbed experiments (Myhre et al., 2017). Richardson et al. (2019) revealed spatial and temporal differences in the surface temperature response to different forcings, such as CO_2 and CH_4, in part due to the physiological CO_2 warming over the densely vegetated regions that is absent under non-CO_2 forcing. This physiological warming occurs because plants close their stomata under elevated CO_2, reducing transpiration and decreasing latent heat loss which causes a local surface warming. Nordling et al. (2021) further demonstrated that the change in long-wave clear-sky emissivity is the key driver of the differences in temperature response between GHGs forcings. Using intermediate-complexity Earth System Climate Model simulations, Nzotungicimpaye et al. (2023) showed that delaying methane mitigation has implications both for meeting the stringent temperature targets and for the climate over many centuries. Using Earth System model simulations, Tokarska et al. (2018) showed that non-CO_2 forcing reduces the remaining carbon budget due to its direct radiative effect on surface temperature, causing additional warming. Fu et al. (2020) showed that non-CO_2 GHGs, which have a shorter atmospheric lifetime than CO_2, may have long-term consequences on climate through their impacts on the carbon cycle. Namely, warming from non-CO_2 GHGs weakens land and ocean carbon sinks.

The weakening of land and ocean carbon sinks due to non-CO_2 GHGs underscores the importance of understanding the differences in carbon cycle feedbacks between CO_2 and non-CO_2 GHGs. Only the changes in CO_2 concentrations give rise to the carbon-concentration feedback, that is the response of the land and ocean carbon uptake to the changes in CO_2 concentration, mainly via the stimulation of photosynthesis by the CO_2 fertilisation effect on land and the solubility pump in the ocean. The changes in both CO_2 and non-CO_2 concentrations lead to the carbon-climate feedback (γ), that is the response of the land and ocean carbon uptake to climate change, mainly via the increased plant and soil respiration over land and reduction of the CO_2 solubility in the ocean with warming (Arora et al., 2013; Schwinger et al., 2014; Zickfeld et al., 2011). Under changing CO_2 concentrations, land and ocean carbon storages respond to both carbon-concentration and carbon-climate feedbacks. However, the interaction between these feedbacks can introduce a non-linearity into the system, whereby the combined effect is not simply the sum of the individual feedbacks (Schwinger et al., 2014; Zickfeld et al., 2011). Thus, temperature-mediated feedback can differ under changing versus constant CO_2 levels, an important distinction when comparing CO_2 and non-CO_2 GHG feedback mechanisms. Here, it is also important to recognize that other factors, such as time lags and potential irreversibilities in the climate system, may also contribute to these differences (Boucher et al., 2012; Chimuka et al., 2023; Schwinger et al., 2014).

Previous studies investigated the nonlinearities in the carbon cycle feedback, showing that the cross term—arising from interactions between changing atmospheric CO_2 and temperatures—can be comparable in size with γ (Schwinger et al., 2014; Zickfeld et al., 2011). They attributed the nonlinearity to the different responses of the land biosphere to the temperature changes, depending on the presence or absence of the CO_2 fertilisation effect, as well as the weakening of ocean circulation and mixing between water masses of different temperatures. However, these studies did not consider non-CO_2 GHGs.

Previous studies have also examined the impact of declining atmospheric CO_2 concentration on the climate and carbon cycle (Boucher et al., 2012; Chimuka et al., 2023; Jones et al., 2016; Koven et al., 2023; Melnikova et al., 2021; Schwinger and Tjiputra, 2018). During the period of decreasing atmospheric CO_2 concentration and temperature (ramp-down), the β and γ feedbacks arise from both the reduction in CO_2 levels and temperature and the inertia of the carbon cycle—specifically, the altered land and ocean carbon pools resulting from prior increases in the CO_2 concentration and temperature (Chimuka et al., 2023; Zickfeld et al., 2016). Melnikova et al. (2021) showed that this leads to an amplification of the β and γ feedbacks under decreasing CO_2 concentration and temperature. The effectiveness of non-CO_2 mitigation has been explored and is an integral part of the integrated assessment models (Ou et al., 2021; Rao and Riahi, 2006; Tanaka et al., 2021). However, few studies investigated the effects of declining non-CO_2 GHG concentrations on the climate and carbon cycle using Earth System Models (ESMs). Abernethy et al. (2021) used an ESM to demonstrate the effectiveness of methane removal in reducing global mean surface temperature, complementing negative CO_2 emissions. Thus, the purpose of this study is twofold:

− to clarify whether the climate and carbon cycle responses to declining CO_2 and non-CO_2 GHGs differ globally and regionally

− to investigate the nonlinearities of carbon cycle feedbacks under CO_2 and non-CO_2 GHG decrease, and the implications for climate change mitigation.

Here, we conduct a series of idealised CO_2 and non-CO_2 (CH_4 and N_2O) concentration-driven ramp-up and ramp-down experiments using the IPSL-CM6A-LR ESM. We then compare the global and spatial impacts of CO_2 and non-CO_2
100 concentration changes on climate and the carbon cycle under overshoot pathways.

2 Data and Methods

2.1 Recalibration of model's CH_4 and N_2O concentrations

We use Version 6 of the Institut Pierre-Simon Laplace (IPSL) low-resolution ESM, IPSL-CM6A-LR (Boucher et al., 2020), developed in the runup to the sixth phase of the Coupled Model Intercomparison Project (CMIP). It comprises the LMDZ
105 atmospheric model Version 6A and the ORCHIDEE land surface model Version 2.0 with a 144×143 spatial resolution, and the NEMO oceanic model Version 3 with a resolution of 1°.

Previous studies showed that IPSL-CM6A-LR can adequately estimate the ERF of CO_2 (Lurton et al., 2020). However, it underestimates the CH_4 radiative forcing for the historical period due to known limitations in the parameterization of gaseous optical properties in the Rapid Radiative Transfer Model (see Fig. 8 in Hogan and Matricardi (2020)). CH_4 also absorbs in the
110 shortwave spectrum, an effect that is not accounted for in the radiative transfer code used in IPSL-CM6A-LR and many other climate models. The Intergovernmental Panel on Climate Change (IPCC) Sixth Assessment Report (AR6) (Forster et al., 2021) estimated the CH_4 ERF to be 0.54 [0.43 to 0.65] W m^{-2} for the 1750–2019 period. However, the estimated ERF of CH_4 at the top of the atmosphere (TOA) in IPSL-CM6A-LR is only 0.27 Wm^{-2} for the 1850–2014 period. Note that in the above estimates, the ERF is defined as the difference in the net TOA flux between a model experiment with perturbed GHG concentration but
115 fixed sea surface and ice temperatures and a control simulation with pre-industrial GHG concentrations. Thus, the estimates include (minimal) effects on the ERF from changes in land surface temperature because, unlike sea surface temperature, the land surface temperature is not prescribed (see Thornhill et al., (2021)). Likewise, the ERF of N_2O may not be accurate in the model. This problem may not be specific to IPSL-CM6A-LR: other climate models (e.g., CNRM-CM6) share the same radiative transfer code and most radiative transfer models used in some climate models have some degree of inaccuracy
120 because they are designed to be computationally efficient (Collins et al., 2006; Fyfe et al., 2021; Pincus et al., 2016). Thus, there is a need to represent the ERF of CH_4 and N_2O more accurately in order to better understand the effects of non-CO_2 GHGs mitigation on the Earth system. As developing better parameterizations of the gaseous optical properties is beyond the scope of this study, we have developed an approach that adjusts CH_4 and N_2O concentrations to 'effective' concentrations that generate CH_4 and N_2O ERFs consistent with the reference estimates of IPCC AR6 (see Appendix A). The effective
125 concentrations of CH_4 and N_2O are used as input to the radiative transfer scheme of the climate model throughout the rest of this study. In the text and figures, these are presented as the actual (equivalent) concentrations.

2.2 Experiment design

We perform and analyse a series of idealised global mean CO_2 and non-CO_2 concentration-driven ensemble experiments as summarised in Table 1 and Fig. 1. Including 50-year ramp-up, ramp-down, and stabilisation periods allows for the exploration of responses to increasing or decreasing CO_2 and non-CO_2 (CH_4 and N_2O) concentrations, as well as the long-term consequences and reversibility of their impacts on the climate and the carbon cycle. The inclusion of CO_2 and non-CO_2 concentration-driven experiments—[CO_2] and [nonCO_2] (with comparable ERF levels), a combined CO_2 and non-CO_2 concentration-driven experiment [CO_2 + nonCO_2], a biogeochemically coupled (BGC) experiment where CO_2 forcing affects only the carbon cycle of land and ocean [CO_2bgc] (with minor temperature effects from CO_2 physiological forcing), and a radiatively coupled (RAD) experiment that includes only CO_2 radiative forcing [CO_2rad] (where CO_2 change does not affect the carbon cycle), enables exploring the impacts of different forcing components on the climate and carbon cycle as well as potential nonlinearities of feedbacks. Additionally, an experiment that combines nonCO_2 radiative forcing with CO_2 physiological forcing [CO_2bgc + nonCO_2] allows for the comparison of nonlinearities arising from combined carbon-concentration feedback and CO_2- and non-CO_2-driven carbon-climate feedback. It serves as the nonCO_2 counterpart of the [CO_2] experiment.

Table 1. Description of experiments. Note that all experiments are analysed relative to their [piControl] counterparts.

Experiment name	Description	Maximum ERF*	Included carbon cycle terms from Eq.2
[CO_2]	0.7% CO_2 concentration increase per year from piControl for 50 years followed by 0.7% CO_2 decrease for 50 years. After CO_2 level returns to piControl, 50 years of stable piControl CO_2 concentrations.	1.88 W m^{-2}	ΔU_β, $\Delta U_{\gamma,CO2}$, $\Delta U_{\chi,CO2}$
[nonCO_2]	2% CH_4 and 2% N_2O concentration increase per year from piControl for 50 years followed by 2% CH_4 and 2% N_2O decrease for 50 years. After CH_4 and N_2O levels return to piControl, 50 years of stable piControl CH_4 and N_2O concentrations.	1.83 W m^{-2}	$\Delta U_{\gamma,nonCO2}$
[CO_2 + nonCO_2]	Combined [CO_2] and [nonCO_2].	3.69 W m^{-2}	ΔU_β, $\Delta U_{\gamma,CO2+nonCO2}$, $\Delta U_{\chi,CO2+nonCO2}$
[CO_2bgc]	Biogeochemically coupled [CO_2].		ΔU_β
[CO_2rad]	Radiatively coupled [CO_2].		$\Delta U_{\gamma,CO2}$
[CO_2bgc + nonCO_2]	[CO_2bgc] and [nonCO_2] combined.		ΔU_β, $\Delta U_{\gamma,nonCO2}$, $\Delta U_{\chi,nonCO2}$
Combinations of experiments			
[CO_2] – [CO_2bgc]	Combination for comparison with [CO_2rad]		$\Delta U_{\gamma,CO2}$, $\Delta U_{\chi,CO2}$
[CO_2bgc + nonCO_2] – [CO_2bgc]	Combination for comparison with [nonCO_2]		$\Delta U_{\gamma,nonCO2}$, $\Delta U_{\chi,nonCO2}$
[CO_2] + [nonCO_2]	Combination for comparison with [CO_2 + nonCO_2]		ΔU_β, $\Delta U_{\gamma,CO2}$, $\Delta U_{\chi,CO2}$, $\Delta U_{\gamma,nonCO2}$

145

The experiment design uses a fixed land cover and constant (other than CO_2, CH_4 and N_2O) GHG and aerosol forcings that might otherwise interfere with the interpretation of the results. The maximum ERF in our experiments is 3.69 W m^{-2}, as estimated from the equations by Etminan et al. (2016) (see also Appendix A), corresponding to (actual) CO_2 concentration of 403 ppm, CH_4 concentration of 2175 ppb and N_2O concentration of 735 ppb. This ERF level (very much in line with the

150   current CO_2 concentration level of ca. 420 ppm) makes our experiments and results relevant to mitigation efforts in the near future. The small differences in ERF between the [CO_2] and [$nonCO_2$] experiments are not significant when considering ramp-up, ramp-down and full periods at $p < 0.05$.
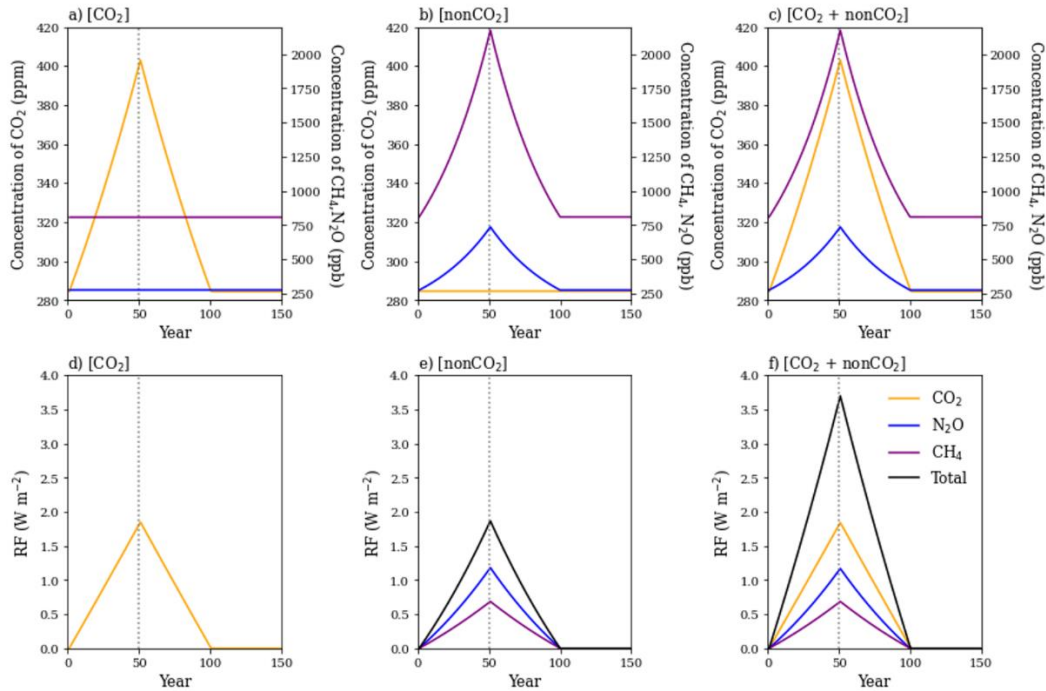
Figure 1: Time series of input (a-c) CO_2, CH_4 and N_2O concentrations and (d-f) their respective radiative ERFs according to Etminan
155   **et al. (2016) equations for (a, d) [CO_2], (b, e) [$nonCO_2$] and (c, f) [CO_2 + $nonCO_2$] experiments. Note the different scales on the *y*-axes in panels a-c for CO_2 concentrations in ppm (left) and other GHG concentrations in ppb (right).**

We investigate CO_2 and non-CO_2 impacts on the climate by looking at the differences between [CO_2] and [$nonCO_2$] experiments and [CO_2rad] and [$nonCO_2$] experiments, hereafter referred to as [CO_2] – [$nonCO_2$] and [CO_2rad] – [$nonCO_2$], respectively. The experiments manipulate CH_4 and N_2O concentrations simultaneously because our primary focus is to

160   compare the effects of CO_2 with those of non-CO_2 gases (i.e., CH_4 and N_2O combined) in this study.

For each experiment, three ensemble members are branched from the years 1870, 2020, and 2170 of the CMIP6 piControl experiment, hereafter [piControl]. We note that the use of three members is not ideal, but it is a common compromise between

computational cost and sampling the uncertainty due to climate variability. We estimate the changes relative to the corresponding [piControl] periods in order to avoid the effects of low-frequency internal climate variability from the piControl

165 (Fig. S1), as discussed in Bonnet et al. (2021). When reporting carbon sink/source in the following sections, we refer to the fluxes relative to the [piControl]. For diagnosing Atlantic Meridional Overturning Circulation (AMOC), we utilised the ocean overturning mass streamfunction in depth space (*msftyz* variable in CMIP6). Specifically, we calculated the maximum annual mean value of the streamfunction in the Atlantic basin north of 20°N through all model's depth layers (up to ca. 5800 m).

2.3 Carbon cycle feedback attribution

170 Traditionally, carbon cycle feedback analysis relies on fully coupled [CO2], biogeochemically-coupled [CO2bgc] and radiatively-coupled [CO2rad] simulations (Arora et al., 2013, 2020; Friedlingstein et al., 2006; Gregory et al., 2009; Schwinger et al., 2014; Schwinger and Tjiputra, 2018; Williams et al., 2019; Zickfeld et al., 2011). The carbon uptake (ΔU) can then be derived using the well-established carbon cycle feedback framework as a sum of carbon-concentration β parameter (GtC ppm^{-1}) multiplied by the changes in the atmospheric CO_2 concentration ΔC_{CO2} (ppm) and carbon-climate γ feedback parameter (GtC

175 K^{-1}) multiplied by the changes in surface temperature ΔT (K), using Eq. (1):

$$\Delta U = \beta \times \Delta C_{CO2} + \gamma \times \Delta T + \varepsilon . \tag{1}$$

Here, term ε refers to a residual term.

The β parameter can be estimated from the [CO2bgc] - [piControl], using Eq. (2):

$$\beta = \frac{\Delta U_{BGC}}{\Delta C_{CO2}}, \tag{2}$$

180 where ΔU_{BGC} is the carbon uptake in the BGC experiment [CO2bgc]. The β feedback reflects the changes in land and ocean carbon pools driven by the changes in CO_2 concentrations.

The γ parameter can be estimated from the [CO2rad] - [piControl], using Eq. (3:

$$\gamma = \frac{\Delta U_{RAD}}{\Delta T}, \tag{3}$$

where ΔU_{RAD} is the carbon uptake in the RAD experiment [CO2rad]. The γ feedback reflects the changes in the land and ocean

185 carbon pools due to the changes in climate.

Many existing studies have estimated γ using the difference between the fully-coupled (COU) and BGC experiments, as a proxy for the RAD experiment (Arora et al., 2013, 2020; Asaadi et al., 2024; Friedlingstein et al., 2003, 2006; Melnikova et al., 2021). However, Zickfeld et al. (2011) and Schwinger et al. (2014) have shown that this substitution introduces a residual term ε, which can be derived from the difference between [CO2] – [CO2bgc] and [CO2rad] - [piControl], using Eq. (4):

190 $$\varepsilon = \Delta U_{COU} - \Delta U_{BGC} - \Delta U_{RAD}. \tag{4}$$

These studies indicate that the residual 'nonlinearity' term depends on both CO_2 concentration and climate change, and it can be of the same order of magnitude as the γ term. Here, we propose that this residual nonlinearity be attributed to a cross term, χ. Although recent studies continue to subsume χ under the γ feedback—partly due to the absence of the [CO2rad] experiment in some experimental designs, and also because this approach has been widely established in earlier research (Friedlingstein

195   et al., 2003, 2006)—we show that these metrics become less well defined when examining the effects of both CO_2 and non-CO_2 GHGs on the carbon cycle.

In order to investigate the associated carbon-climate feedback nonlinearities, we propose the following theoretical framework. The changes in carbon uptake $\Delta U(\Delta C_{co2}, \Delta T)$ (GtC year^{-1}) in the COU simulation can be defined as a function of changes in CO_2 concentration (ΔC_{CO2}) and temperature (ΔT). Following Schwinger et al. (2014), the formulation can be expanded to a

200   Taylor series up to the second-order terms:

$$\Delta U = \Delta U(\Delta C_{co2}, \Delta T) = \frac{\partial U}{\partial C_{CO2}}\Delta C_{co2} + \frac{\partial U}{\partial T}\Delta T + \frac{\partial^2 U}{\partial C_{CO2}\,\partial T}\Delta T\Delta C_{co2} + \frac{1}{2}\frac{\partial^2 U}{\partial C_{CO2}^2}(\Delta C_{co2})^2 + \frac{1}{2}\frac{\partial^2 U}{\partial T^2}(\Delta T)^2 + Res. \tag{5}$$

where ΔC_{CO2} and $\Delta T_{forc.}$ are the respective increments of CO_2 concentration and temperature relative to [piControl]. The third and higher order terms are defined as a residual ($Res.$). We found them to be negligible in our case. We can disentangle the

205   first- and second-order terms of the right-hand side of the Eq. (5) into terms that are purely dependent on CO_2 (ΔU_β), on temperature (ΔU_γ) and the cross term (ΔU_χ), as follows:

$$\Delta U_\beta = \frac{\partial U}{\partial C_{CO2}}\Delta C_{CO2} + Res., \tag{6}$$

$$\Delta U_\gamma = \frac{\partial U}{\partial T}\Delta T + Res., \tag{7}$$

210     $$\Delta U_\chi = \frac{\partial^2 U}{\partial C_{CO2}\,\partial T}\Delta T\Delta C_{CO2} + Res.. \tag{8}$$

For simplicity, the second-order terms of Eqs. (6) and (7) are included in $Res.$. Combining Eqs. (4) and (8), the χ feedback parameter may be quantified from:

$$\chi = \frac{\Delta U_{COU-BGC} - \Delta U_{RAD}}{\Delta T\Delta C_{CO2}}. \tag{9}$$

215   The carbon-concentration β feedback term ΔU_β may be estimated from [CO_2bgc] - [piControl], under the assumption that the physiological CO_2 warming and its impacts on the carbon cycle are negligible, consistent with findings of Asaadi et al., (2024). The γ feedback terms for CO_2 ($\Delta U_{\gamma,CO2}$) and non-CO_2 ($\Delta U_{\gamma,nonCO2}$) gases are estimated from [CO_2rad] - [piControl], and [nonCO_2] - [piControl], respectively. The difference between these terms ($\Delta U_{\gamma,CO2} - \Delta U_{\gamma,nonCO2}$) yields the difference between impacts of CO_2 and non-CO_2 forcing on the carbon-climate feedback. Finally, the cross term ΔU_χ, previously referred

220   to as nonlinearity term (Arora et al., 2013, 2020; Gregory et al., 2009; Schwinger et al., 2014; Schwinger and Tjiputra, 2018; Williams et al., 2019; Zickfeld et al., 2011), may be estimated by utilising a combination of experiments. The combination [CO_2] – [CO_2bgc] - [CO_2rad] gives $\Delta U_{\chi,CO2}$, and the combination [CO_2bgc + nonCO_2] – [CO_2bgc] - [nonCO_2] gives $\Delta U_{\chi,nonCO2}$). Analogously, the difference between these cross terms ($\Delta U_{\chi,CO2} - \Delta U_{\chi,nonCO2}$) yields the difference between the CO_2 and non-CO_2 forcings on the χ.

3 Results and discussion

3.1 Climate impacts

The analysis of global climate variables as a function of CO_2 concentration and GSAT shown in Fig. 2 follows a previous study by Boucher et al. (2012). Consistent with their findings, our results show that GSAT change lags behind GHG forcing by up to a decade. The lag increases with the increase in the forcing magnitude, so that the largest lag is in the [CO_2 + nonCO_2] experiment. Even after a ramp-down period and 50 years of constant GHG forcing at [piControl] levels, GSAT does not return to preindustrial values in all experiments (Fig. 2a). This can be explained by the inertia of the climate system, apparent in the changes in the ocean heat uptake (OHU). The OHU increases during the ramp-up and decreases during the ramp-down period, being positive, i.e., taking up energy away from the atmosphere, during the ramp-up and first half of the ramp-down period. OHU turns negative by the end of the ramp-down and stays negative during the 50 years of the stabilisation period, releasing energy back into the atmosphere (Fig. 2c-e). The hysteresis of the climate system is evident from the nearly linear relationship between maximum GSAT and mean GSAT during the stabilisation period (Fig. S2). The thermosteric (unrelated to ice sheet melting) sea level increases in all experiments except for [CO_2bgc] and is closely related to the OHU. It does not recover (i.e. it is irreversible) within the time-horizon considered here (Fig. 2 i-k). The AMOC decreases with GSAT (with the strongest decrease reached for GSAT = 2 °C under [CO_2 + nonCO_2]), but fully recovers (Fig. S1b).
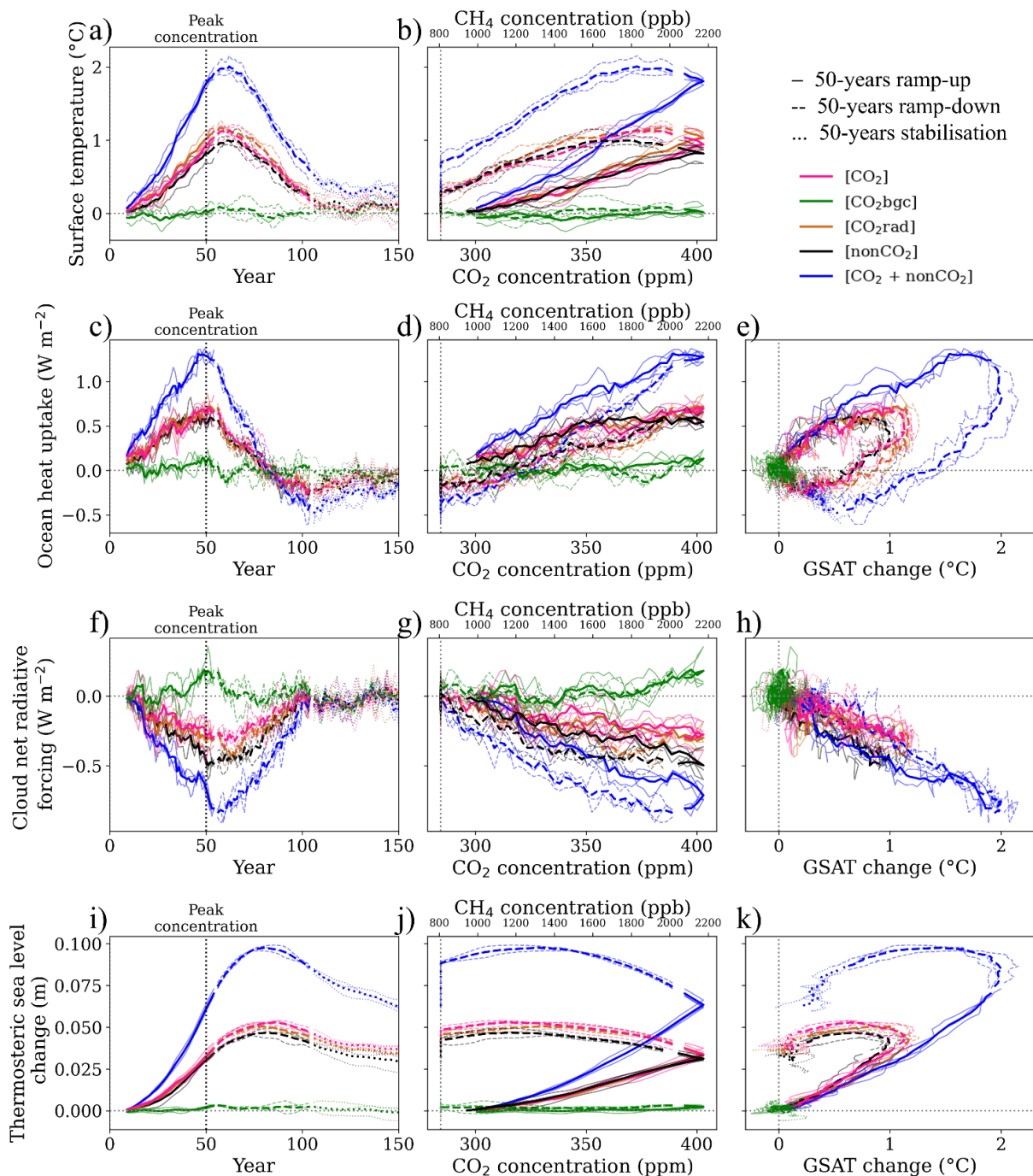
Figure 2: Global annual mean changes in model climate variables as a function of (a, c, f, i) time (year), (b, d, g, j) CO₂ concentration (ppm) / CH₄ concentration (ppb, only for [nonCO2]), (c, e, h, k) GSAT (°C) for (a, b) GSAT (°C), (c–e) ocean heat uptake (W m⁻²), (f–h) cloud net radiative forcing (W m⁻²), and (i–k) thermosteric sea level change (m) under selected scenarios. The ramp-up, ramp-down and stabilisation periods are indicated by different line styles in all panels. Thick lines indicate the ensemble means and thin lines correspond to three ensemble members.

The CO$_2$ physiological warming that can be quantified by comparing [CO$_2$bgc] with [piControl] is small (green line in Fig. 2). Spatially, some differences are ubiquitous over land, e.g., CO$_2$ physiological warming persists over Eurasia during the ramp-up period, and over the high latitudes of both land and ocean during the stabilisation period (Fig. S3a). A larger ensemble size of model simulations would be required to investigate these differences more thoroughly. In our following analysis on carbon cycle feedbacks, we assume the CO$_2$ physiological warming to be negligible, consistent with previous findings of Asaadi et al., (2024).

When comparing CO$_2$- and non-CO$_2$-induced forcing ([CO$_2$] and [nonCO$_2$] experiments) at a global scale, our results are consistent with Richardson et al. (2019) who show the higher surface temperature response of CO$_2$ when compared to CH$_4$. When comparing CO$_2$- and non-CO$_2$-induced radiative forcing ([CO$_2$rad] and [nonCO$_2$] experiments) at a global scale, the non-CO$_2$ forcing still leads to a lower GSAT peak and a slightly lower peak of thermosteric sea level rise compared to the CO$_2$ radiative forcing (brown and black lines of Fig. 2a, significant difference at $p < 0.05$). This cannot be explained just by a slightly higher ERF of the [CO$_2$rad] compared to [nonCO$_2$] experiment (Table 1, Figs. 2a, S4). Our results are consistent with Nordling et al. (2021) who show the higher effective temperature response for CO$_2$ forcing compared to non-CO$_2$ forcing, attributing it to the changes in clear-sky planetary emissivity.

Radiative forcing alone ([CO$_2$rad] experiment) leads to a slightly higher global temperature increase compared to the coupled [CO$_2$] experiment, which includes the combined effect of CO$_2$ physiology and radiative forcing (Fig. 2a, b). This temperature difference is particularly evident in the Arctic region (Fig. S3a). Our findings differ from those of a CMIP5 intercomparison study, which reported that CO$_2$ physiological warming amplifies the Arctic warming (Park et al., 2020). The study showed that the CO$_2$ physiological effect contributes to high latitude warming by reducing evaporative cooling due to stomatal closure under elevated CO$_2$ levels. In contrast, we observe higher evapotranspiration in the [CO$_2$rad] compared to the [CO$_2$] experiment (Fig. S5), which is probably a consequence of the lower warming in the [CO$_2$] experiment. In our study, the greater warming in the [CO$_2$rad] experiment may be driven by increased surface albedo, especially in the Arctic Ocean (Fig. S3b). While the underlying causes remain unclear, this pattern appears consistent in other experiments conducted with IPSL-CM6A-LR under moderate CO$_2$ levels (not shown). Because the ensemble size in our study is limited and the effects of the model's internal variability should be considerable, future research should validate the robustness of our findings with larger ensemble simulations.

3.2 Carbon cycle feedback

3.3 Carbon-concentration feedback

The term $\Delta U_{\beta,CO2}$ corresponds to the flux arising from variations in CO$_2$ concentration ([CO$_2$bgc] experiment). The $\Delta U_{\beta,CO2}$ dominates the land and ocean carbon uptake changes through all three considered periods (Fig. 3, Tables 2, S1). Since the considered maximum surface warming levels are below 2 °C, land and ocean carbon fluxes are primarily controlled by the CO$_2$-induced effects during the ramp-up period, resulting in positive β (Fig. 3 a-d). Nearly two-thirds of land and half of ocean

carbon accumulated during the ramp-up period due to the atmospheric CO_2 increase is being released during the latter periods, consistent with previous studies (Asaadi et al., 2024; Chimuka et al., 2023). In the ocean, β is positive (carbon sink) in all

280 regions during the ramp-up period. However, CO_2 concentration decrease induces carbon source over all ocean regions, except for the Atlantic and Southern Oceans (Fig. 4). All regions are carbon sources during the stabilisation period of the [CO_2bgc] experiment.

285 **Table 2. Cumulative CO_2 and climate change-driven changes in the land and ocean carbon fluxes (GtC), shown as three- member ensemble mean. The ± indicates one standard deviation among the three members. Note that all experiments are analysed relative to their [piControl] counterparts.**

Experiment	Max. warming (K)*	Terms	Years 1-50 (ramp-up)		Years 51-100 (ramp-down)		Years 101-150 (stabilisation)		Total	
			Land	Ocean	Land	Ocean	Land	Ocean	Land	Ocean
[CO_2bgc]	0.1±0.0	$\Delta U_{\beta,CO2}$	179.3±2.2	103.8±0.7	-16.3±6.0	-19.7±1.0	-106.3±0.4	-32.1±0.8	59.4±1.8	53.4±0.9
[CO_2rad]	1.1±0.1	$\Delta U_{\gamma,CO2}$	-18.6±2.4	-2.4±0.2	4.5±5.7	0.0±1.4	11.4±4.0	0.3±1.9	-2.2±2.0	-2.1±0.6
[nonCO_2]	0.9±0.1	$\Delta U_{\gamma,nonCO2}$	-14.8±3.6	-2.3±1.0	1.3±6.0	-0.5±1.3	10.2±2.4	1.3±0.5	-2.5±2.9	-1.6±0.2
[CO_2] − [CO_2bgc]	1.0±0.0	$\Delta U_{\gamma,CO2} + \Delta U_{\chi,CO2}$	-14.7±1.0	-4.5±0.2	3.8±3.0	-1.4±1.0	8.2±1.9	0.6±0.5	-3.8±3.1	-5.5±1.4
		$\Delta U_{\chi,CO2}$	3.9±2.1	-2.2±0.4	-0.7±7.3	-1.4±0.5	-3.2±5.9	0.2±2.3	-1.6±5.0	-3.4±2.0
		$\Delta U_{\chi,nonCO2}$	3.5±1.5	-1.6±1.0	2.8±7.9	0.1±1.1	-1.6±1.5	-1.0±1.3	2.0±4.0	-2.5±1.0
		$\Delta U_{\gamma,CO2} - \Delta U_{\gamma,nonCO2}$	-3.8±5.0	-0.1±0.9	3.2±3.6	0.5±0.9	1.2±2.6	-1.0±2.2	0.3±2.7	-0.5±0.7
		$\Delta U_{\chi,CO2} - \Delta U_{\chi,nonCO2}$	0.4±3.5	-0.6±0.7	-3.5±3.4	-1.6±1.0	-1.6±7.4	1.3±3.3	-3.6±5.5	-1.0±2.8

* defined as the mean ΔGSAT during years 41-60 in the experiments.

The transient change of the β feedback over land can be better explained by analysing the gross primary production (GPP) and

290 the autotrophic and heterotrophic respiration (Ra and Rh) fluxes. Land GPP, representing photosynthetic uptake, increases during the ramp-up period under elevated CO_2 concentration and decreases almost linearly with decreasing CO_2, showing only a small hysteresis (Figs. S6-7). In contrast, both Ra and Rh exhibit a larger hysteresis, which leads to an extended period of the carbon release to the atmosphere. This suggests that while there may be initial carbon sequestration benefits gained during elevated CO_2 periods, these benefits are susceptible to being lost as CO_2 concentrations decline due to decreased photosynthesis

295 and increased respiration, albeit at a reduced rate.

The spatial variation of cumulative net carbon uptake provides further details on the feedback changes (Figs. 4, S8-S10). During the CO_2 ramp-up phase, CO_2 increase triggers a land carbon sink in all regions. However, during the ramp-down phase, it induces a net carbon source over subtropical regions while still driving a land carbon sink in northern high-latitudes, so that global land becomes a carbon source in the middle of the ramp-down phase. Finally, during the stabilisation period, all land

300 regions become net carbon sources.

Subtropical and southern land regions exhibit a shorter hysteresis in response to decreasing CO_2 concentrations. This disparity arises from the larger proportion of carbon accumulated in aboveground vegetation biomass in southern regions, contrasting with the greater fraction stored in soils within northern latitudes (Figs. S9-S11). The extended period of high positive β in northern mid- to high latitudes can be attributed to the longer carbon turnover time, particularly in soils, compared to tropical regions (Fig. S8).

3.4 Carbon-climate feedback

The term ΔU_γ corresponds to the carbon flux arising from variations in radiative forcing (such as in the [nonCO₂] and [CO₂rad] experiments). The ΔU_γ for CO_2 and non-CO_2 ($\Delta U_{\gamma,CO2}$ and $\Delta U_{\gamma,nonCO2}$, respectively) are equivalent (within one standard deviation uncertainty range) under nearly equivalent levels of ERF (compare panels b and c of Fig. 4, see also $\Delta U_{\gamma,CO2} - \Delta U_{\gamma,nonCO2}$ in Table 2, see also Table S1). The γ is negative on a global scale in the land and ocean, with greater magnitude but also faster reversibility over land. Spatially, land γ is positive in the mid- to high latitudes and negative in the tropical regions (Figs. 4, S9-10, see also Melnikova et al. (2021)). During the ramp-up, climate change drives carbon sink in the northern mid- to high- latitudes and carbon source in the subtropical regions and the Southern Hemisphere, with larger magnitude of changes in the experiments, in which CO_2 concentration change is present (Figs. 4, S9-11).
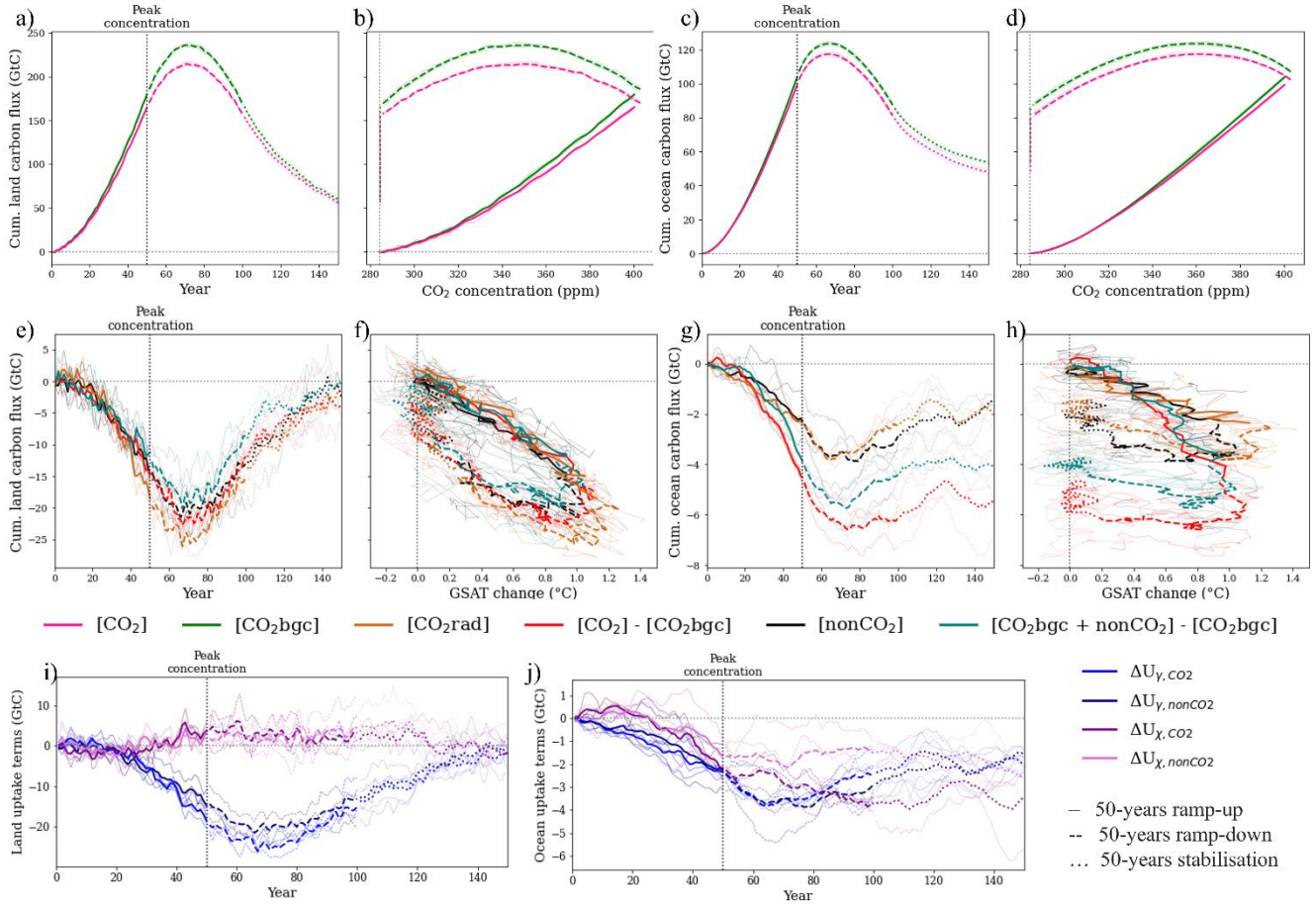
315

Figure 3. Global cumulative carbon fluxes (GtC) over (a, b, e, f, i) land and (c, d, g, h, j) ocean as a function of (a, c, e, g, i, j) time (year), (b, d) CO₂ concentration (ppm) and (f, h) GSAT changes (ºC) under selected scenarios. The ramp-up, ramp-down and stabilisation periods are indicated by different line styles. Thick lines indicate the ensemble means and thin lines correspond to other ensemble members. Note that vertical axes differ between panels e, g and i, j.

320 **3.5 Nonlinearity in carbon cycle feedback**

The cross term ΔU_χ induces non-negligible differences between climate change-induced carbon flux when comparing experiments with presence or absence of atmospheric CO_2 concentration change. It reaches ca. 20–23% of the land ΔU_γ and ca. 70–90% of the ocean ΔU_γ, cumulative over the ramp-up period (Table 2). During the ramp-up phase, the ΔU_χ corresponds to a decrease in the climate-driven land carbon source and an increase in the climate-driven ocean carbon source (Fig. 3). The

325 χ feedback is positive (larger carbon sink) on land and negative (larger carbon source) in the ocean (Table S1). There is no significant difference between CO_2 and non-CO_2 χ feedback at similar ERF levels (Fig. 3e-j, Fig. 4 f-g, Tables 2 and S1). In the ocean, the cross-term differences for CO_2 and non-CO_2 forcing arise already during the ramp-up and propagate during the ramp-down and stabilisation phases, spatially concentrating in the deep mixing region of the Southern Ocean.

On land, the positive χ reflects more biomass at high latitudes available for climate change effects, leading to a larger carbon

330   sink (positive γ). During the ramp-down, climate warming through temperature change (lagged after GHG concentrations change) increases the carbon sink over high latitudes and weakens the carbon source in the tropics. Here the ΔU_χ reflects more biomass available globally for the climate change effects, leading to a larger carbon source (negative γ). The differences (in the presence / absence of the cross term ΔU_χ) diminish for land but not for the ocean during the ramp-down and stabilisation periods.

335   In the ocean, the contribution from the nonlinearity of carbon cycle feedbacks leads to a greater reduction in the CO_2-driven carbon sink (Fig. 3). The contribution of the cross term ΔU_χ to the total ΔU increases during the ramp-down phases of considered GHG concentration scenarios. Previously, Schwinger and Tjiputra (2018), who considered nonlinearity of carbon cycle feedback, warned that RAD experiments may underestimate the carbon-climate feedback (when compared to COU - BGC experiments), because "the reduction of sequestration of preformed dissolved inorganic carbon under high atmospheric

340   CO_2 is not taken into account." In this study, the nonlinearity effects nearly double climate change-driven carbon loss (compared to the RAD experiment, in which atmospheric CO_2 is constant) relative to the total net 150-year net ocean carbon uptake under the [CO_2] experiment. Spatially, while the Southern Ocean remains the largest ocean carbon sink in all considered experiments involving atmospheric CO_2 changes, it, along with the Atlantic Ocean, undergoes the largest climate change-driven reduction in carbon sink (Fig. 4).
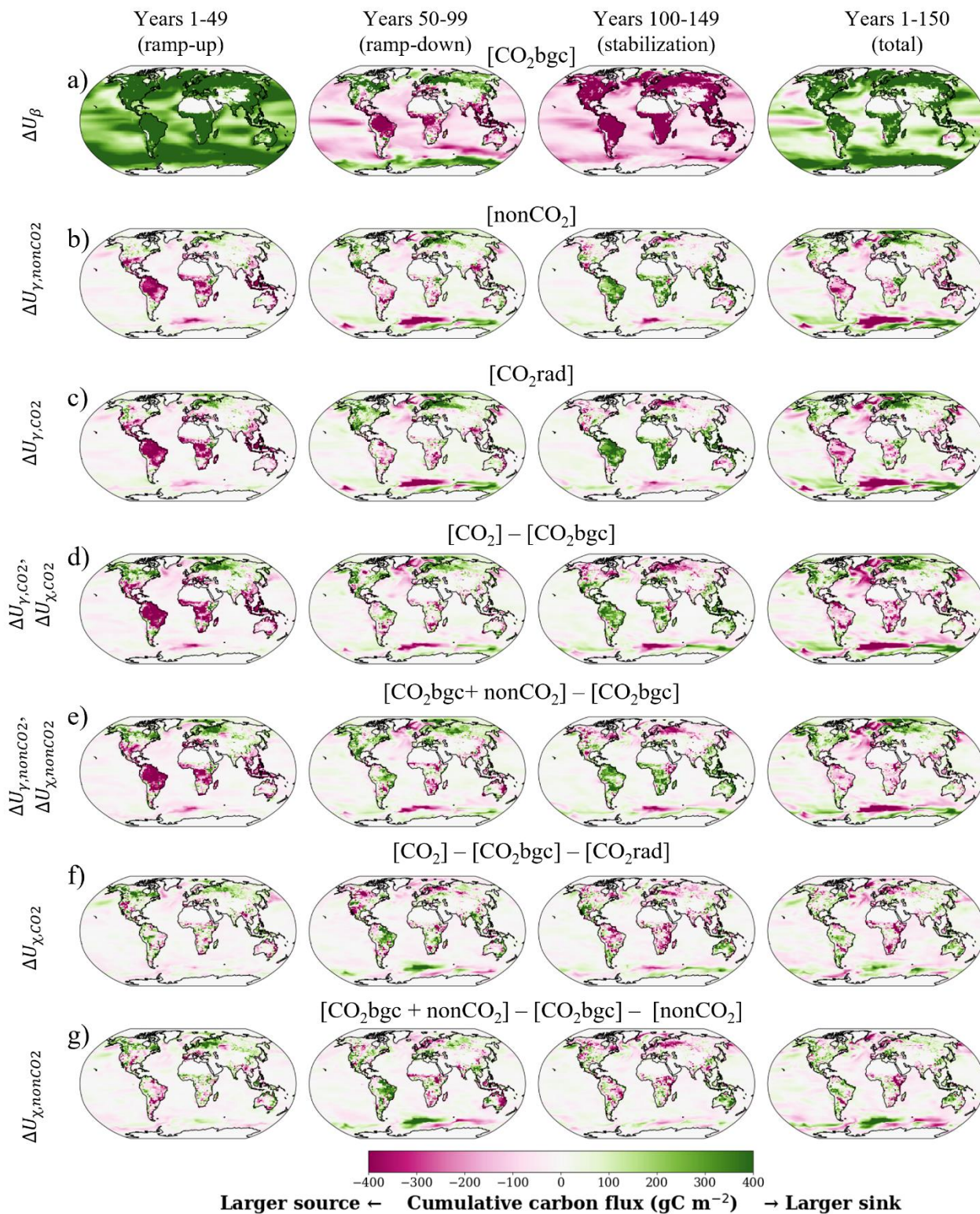
Figure 4. Spatial variation of land and ocean carbon fluxes (GtC, negative to the atmosphere) cumulative over 50 years of (first column) ramp-up, (second column) ramp-down, (third column) stabilisation phases and (last column) full 150-year period. The data for three-member-ensemble mean are used.

Our findings provide evidence on the effectiveness of non-CO_2 GHG mitigation. While it can effectively reduce GSAT peak, non-CO_2 GHG mitigation may also lead to smaller climate change-driven losses in the ocean carbon sink. In the real world, the presence / absence of ΔU_χ suggests disparities between CO_2 mitigation efforts and non-CO_2 mitigation efforts. The CO_2- and non-CO_2-driven climate change leads to unequal decrease in carbon uptake, especially apparent for the ocean on a global scale (compare red and black lines in Fig. 3, corresponding to [CO_2] – [CO_2bgc] and [nonCO_2] experiments). Reducing CO_2 concentrations for climate mitigation implies alteration of all three terms of the proposed carbon cycle feedback attribution framework, namely ΔU_β, ΔU_γ and ΔU_χ. Reducing non-CO_2 GHG concentrations, such as CH_4 and N_2O, implies alteration of ΔU_γ and ΔU_χ terms. Reducing both CO_2 and non-CO_2 concentrations implies alteration of all ΔU_β, ΔU_γ and ΔU_χ terms but with larger change in ΔU_γ and ΔU_χ terms. From this point, combining CO_2 and non-CO_2 reduction measures may be more effective for climate change mitigation, compared to the CO_2 reduction measures alone. This finding should be confirmed with emission-driven experiments that consider GHGs atmospheric lifetimes.

3.6 Radiative forcing and carbon cycle feedback additivity

In order to overcome the small signal-to-noise ratio of the considered experiments as well as the regional differences in the radiative forcing between [CO_2] and [nonCO_2] experiments, we compare the (1) [CO_2 + nonCO_2] experiment that include both CO_2 and non-CO_2 effects with (2) the sum of two [CO_2] and [nonCO_2], that include CO_2 and non-CO_2 effects, accordingly (Figs. 5 and S12-13). The climate effects, defined via temperature change, differ during the ramp-up and ramp-down periods (Fig. S12). These differences imply non-additivity of radiative forcing and can also be attributed to biophysical feedback.

As for the carbon cycle feedback, the [CO_2 + nonCO_2] experiment that has all feedback is different from the sum of two experiments [CO_2] + [nonCO_2] both on land and in the ocean (Fig. 5). The differences are larger and stay longer in the ocean. This implies non-additivity of carbon cycle feedback. From the proposed carbon cycle feedback attribution framework, the non-additivity arises from nonequality of $(\Delta U_{\gamma,CO2+nonCO2} + \Delta U_{\chi,CO2+nonCO2})$ and $(\Delta U_{\gamma,CO2} + \Delta U_{\chi,CO2} + \Delta U_{\gamma,nonCO2} + \Delta U_{\chi,nonCO2})$. The significant difference ($p < 0.1$) on land is in the high-latitude region, where "all-effects together" [CO_2 + nonCO_2] experiment yields a larger carbon sink during the ramp-up phase. The largest difference in the ocean is in the Southern Ocean, followed by the North Atlantic Ocean. The [CO_2 + nonCO_2] experiment has large carbon sink is in the Southern Ocean compared to the sum of two experiments. This might be related to the saturation of the decrease in the mixed layer depth with more warming, but a more thorough study is needed to confirm such phenomena.
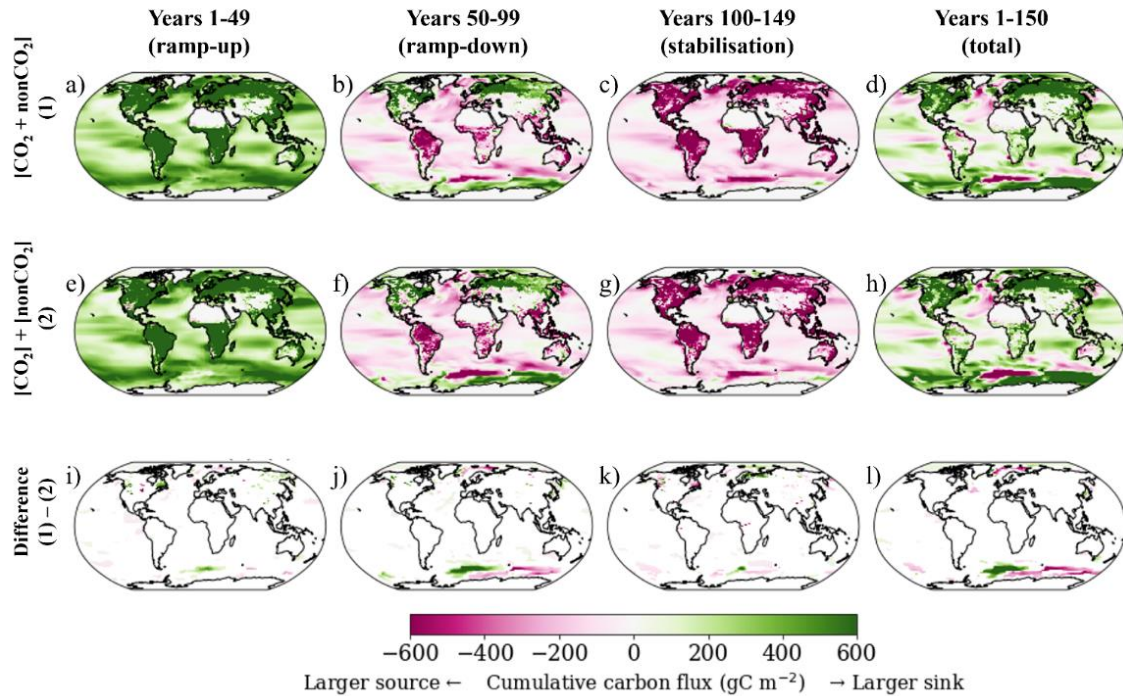
Figure 5. Spatial variation of three-member-ensemble mean land and ocean carbon fluxes (GtC, negative to the atmosphere) cumulative over 50 years of (a, e, i) ramp-up, (b, f, j) ramp-down, (c, g, k) stabilisation phases and (d, h, l) full 150-year period. We draw only significantly different grids between (i-l) [CO$_2$ + nonCO$_2$] and [CO$_2$] + [nonCO$_2$] experiments using three ensemble members ($p < 0.1$ based on t-test, N=60).

4 Limitations and future research directions

To our knowledge, this is the first study of its kind to compare idealised CO$_2$ and non-CO$_2$ ramp-up and ramp-down scenarios for their effects on global temperature change and the carbon-cycle feedbacks. Below we draw attention to the caveats and limitations that should be addressed in future studies.

First, since IPSL-CM6A-LR, like all other ESMs participating in CMIP6, does not have interactive modules of the CH$_4$ and N$_2$O cycles, the changes in stratospheric water vapour, aerosols, and tropospheric ozone due to atmospheric CH$_4$ changes, as well as the effects of nitrogen deposition on the carbon cycle are not considered in this study. Future studies could consider simulations separately for CH$_4$ and N$_2$O. However for this study, the use of the model is justified because current changes in CH$_4$ and N$_2$O concentrations are primarily driven by anthropogenic sources, suggesting that the absence of interactive modules of natural sink/source processes does not significantly affect the representation of natural variability trends for the CH$_4$ and N$_2$O concentration (Nakazawa, 2020; Palazzo Corner et al., 2023; Zhu et al., 2013).

Second, when interpreting the results, it should be kept in mind that some carbon cycle processes in IPSL-CM6A-LR such as permafrost and fire are not considered. Yet, these should have only a limited impact on our results, given the (relatively) small

warming levels in the considered experiments. Previous studies have shown that IPSL-CM6A-LR estimates one of the smallest soil carbon pools among CMIP6 models, which may lead to an underestimation of the carbon-climate feedback (Arora et al., 2020; Melnikova et al., 2021).

Third, the results of the present study are limited by the use of a single ESM and a small number of ensemble members. Conducting similar experiments with other ESMs and using larger ensemble runs, which are particularly valuable in the low warming scenarios, as well as complementing the findings of our study with emission-driven experiments, could contribute to validating and extending our findings.

5 Conclusions

This study first presents a novel approach to recalibrate the ERF of CH_4 and N_2O in ESMs without changing the radiative scheme of the model. We then discuss the effects of increases and decreases in the concentrations of the CO_2 and non-CO_2 GHGs on the surface climate and carbon cycle. We find only small differences between CO_2 and non-CO_2 ramp-up and ramp-down forcing on global and regional climate.

The differences in climate responses can be linked to differences in the carbon cycle feedbacks. We show that CO_2- and non-CO_2-driven carbon-climate feedback are nearly equivalent at a global scale. However, increasing atmospheric CO_2 amplifies the reduction of the climate change-driven carbon sink, especially in the ocean. We propose a novel framework to disentangle the carbon-climate feedback into a component that is purely driven by climate change i.e., expressed as a temperature term, and a component driven by climate change and rising atmospheric CO_2 at the same time, i.e., a cross term. Since the cross term can be quantified from the difference between COU, BGC and RAD simulations, we advocate for continuing to carry out all three types of experiments in the future phases of CMIP. We further warn that the cross term and non-additivity of feedback should be considered in the simple climate models (emulators).

Finally, this study showcases the additional benefits of non-CO_2 GHG mitigation on a smaller reduction of the ocean carbon sinks under overshoot scenarios. We stress that our findings do not imply that non-CO_2 GHG mitigation should be given a priority over other means to mitigate climate change but they provide an insight on the intricate interplay between the carbon-concentration and CO_2- and non-CO_2-driven carbon-climate feedbacks to inform comprehensive mitigation strategies.

Appendix A

A set of 40-year idealised IPSL-CM6A-LR simulations (840 years in total) has been carried out. In these experiments, the sea surface temperature (SST) and sea ice fractions were fixed to their preindustrial levels. CH_4 concentration levels were kept at $2 \times CH_4$, $3 \times CH_4$, $4 \times CH_4$, $5 \times CH_4$, $8 \times CH_4$, and $12 \times CH_4$, and N_2O concentration levels were kept at $1 \times N_2O$, $1.25 \times N_2O$, $1.5 \times N_2O$, and $1.75 \times N_2O$ (Table A1).

Table A1. Description of idealised recalibration experiments using IPSL-CM6A-LR

№	Name	Concentration		
		CH$_4$ (ppb)	N$_2$O (ppb)	CO$_2$ (ppm)
0	*piClim*	808.25	273.02	284.32
1	2×CH$_4$	1616.50	273.02	284.32
2	3×CH$_4$	2424.75	273.02	284.32
3	4×CH$_4$	3233.00	273.02	284.32
4	5×CH$_4$	4041.25	273.02	284.32
5	8×CH$_4$	6466.00	273.02	284.32
6	12×CH$_4$	9699.00	273.02	284.32
7	1×CH$_4$-1d25N$_2$O	808.25	341.28	284.32
8	2×CH$_4$-1d25N$_2$O	1616.50	341.28	284.32
9	3×CH$_4$-1d25N$_2$O	2424.75	341.28	284.32
10	4×CH$_4$-1d25N$_2$O	3233.00	341.28	284.32
11	5×CH$_4$-1d25N$_2$O	4041.25	341.28	284.32
12	8×CH$_4$-1d25N$_2$O	6466.00	341.28	284.32
13	12×CH$_4$-1d25N$_2$O	9699.00	341.28	284.32
14	1×CH$_4$-1d5N$_2$O	808.25	409.53	284.32
15	2×CH$_4$-1d5N$_2$O	1616.50	409.53	284.32
16	3×CH$_4$-1d5N$_2$O	2424.75	409.53	284.32
17	4×CH$_4$-1d5N$_2$O	3233.00	409.53	284.32
18	5×CH$_4$-1d5N$_2$O	4041.25	409.53	284.32
19	8×CH$_4$-1d5N$_2$O	6366.00	409.53	284.32
20	12×CH$_4$-1d5N$_2$O	9699.00	409.53	284.32
21	1×CH$_4$-1d75N$_2$O	808.25	477.79	284.32

Fig. A1 shows the set of 40-year time series of global mean radiative forcing based on 21 idealised experiments. The *piClim*
425   experiment holds pre-industrial levels of CO$_2$, CH$_4$ and N$_2$O concentrations. The mean interannual variation of the radiative
forcings (one standard deviation) is 0.15 Wm^{-2}. The first 10 years of the experiments were dropped to allow the climate to
adjust to the new radiative equilibrium after an abrupt change from the pre-industrial levels. The last 30 years were used to
obtain eighteen data-points of mean global ERF by IPSL-CM6A-LR relative to the levels obtained from the *piClim* experiment.
The ERF is estimated as a TOA imbalance difference between each experiment and the *piClim*.
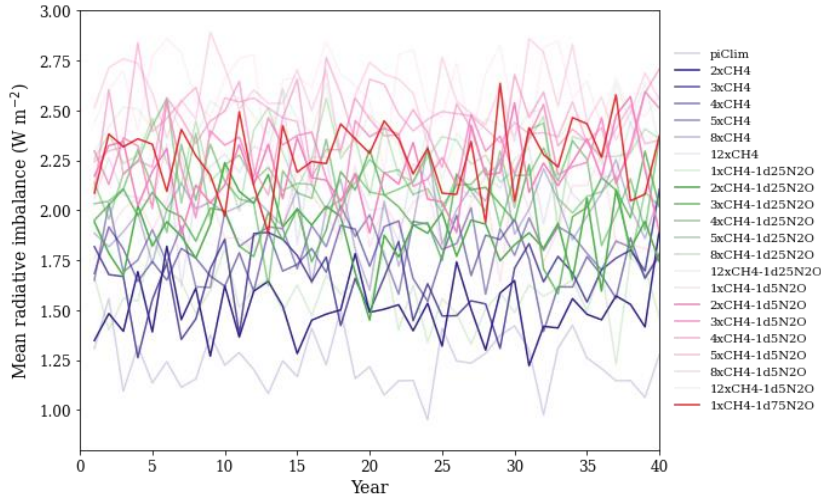
430

Figure A1. Time series of global mean radiative imbalance of IPSL-CM6A-LR idealised experiments

There are two frequently used sets of equations to derive radiative forcing of well mixed greenhouse gases, e.g., CO_2, CH_4 and N_2O, etc., based on their concentrations. The first set from Myhre et al. (Myhre et al., 1998), thereafter, M98, was used in IPCC AR3:

$$RF(CO2) = 5.35 \times ln\,(CO2/CO2_{t=0})$$

$$RF(CH4) = 0.036 \times (\sqrt{CH4} - \sqrt{CH4_{t=0}}) - (f(CH4, N2O_{t=0}) - f(CH4_{t=0}, N2O_{t=0}))$$

$$RF(N2O) = 0.12 \times \left(\sqrt{N2O} - \sqrt{N2O_{t=0}}\right) - (f(CH4_{t=0}, N2O) - f(CH4_{t=0}, N2O_{t=0}))$$

(A1)

$$f(CH4, N2O) = 0.47 \times ln[1 + 2.01 \times 10^{-5} \times (CH4 \times N2O)^{0.75} + 5.31 \times 10^{-15} \times CH4 \times (CH4 \times N2O)^{1.52}]$$

435 Here the CO_2, CH_4 and N_2O indicate their concentrations, where the units are ppm, ppb, and ppb.

Etminan et al. (2016), thereafter, E16, improved the IPCC AR3 equations by inclusion of the shortwave (near-infrared) bands of CH_4. Their set of equations was used in IPCC AR6. The radiative forcing of N_2O in the M98 equation depends on the CH_4 and N_2O concentrations, while the radiative forcing of N_2O in the equation by E16 depends on the CO_2, CH_4 and N_2O concentrations:

$$RF(CO2) = [-2.4 \times 10^{-7} \times (CO2 - CO2_{t=0})^2 + 7.2 \times 10^{-4} \times |CO2 - CO2_{t=0}|$$
$$-\,2.1 \times 10^{-4} \times \frac{1}{2}(N2O + N2O_{t=0}) + 5.36]\,ln\,(\frac{CO2}{CO2_{t=0}})$$

$$RF(CH_4) = \left[-1.3 \times 10^{-6} \times \frac{1}{2}(CH4 + CH4_{t=0}) - 8.2 \times 10^{-6} \times \frac{1}{2}(N2O + N2O_{t=0}) + 0.043\right] \times (\sqrt{CH4}$$
$$-\,\sqrt{CH4_{t=0}})$$

(A2)

$$RF(N_2O) = [-8.0 \times 10^{-6} \times \frac{1}{2}(CO2 + CO2_{t=0}) + (4.2 \times 10^{-6} \times \frac{1}{2}(N2O + N2O_{t=0})$$

$$- 4.9 \times 10^{-6} \times \frac{1}{2}(CH4 + CH4_{t=0}) + 0.117] \times (\sqrt{N2O} - \sqrt{N2O_{t=0}})$$

440 In the sets of Eqs. (A2), the radiative forcing due to CH_4 depends not only on the CH_4 concentration but also on that of N_2O (and conversely) because CH_4 and N_2O absorption bands overlap to some extent. These simplified equations are therefore additive: the radiative forcing due to a change in CH_4 and N_2O concentrations (CH_4, N_2O) relative to reference (preindustrial) values ($CH4_{t=0}$, $N2O_{t=0}$) is equal to:

$$RF(CH4, N2O) = RF_{CH4}(CH4, N2O) + RF_{N2O}(H4, N2O) \tag{A3}$$

445 The effect of CO_2 on the radiative forcing of N_2O is small (<5%), and thus, for simplicity, is neglected in the rest of this study (Fig. A2).
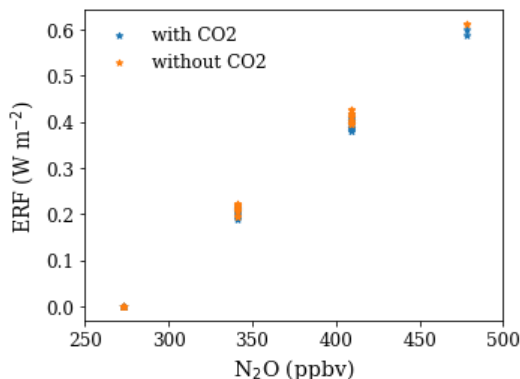
Figure A2.The ERF estimated from E16 with and without accounting for CO₂ impact on the N₂O forcing (including/excluding the term $-8.0 \times 10^{-6} \times 0.5 \times (CO_2 + CO_{2,t=0})$ in the equation) using the concentration values of the idealised experiments described
450 **in the Table 1 with preindustrial CO₂ concentration (284.32 ppm) and the same set of the experiments with 3 × CO₂ concentration (852.96 ppm).**

Figure A3 shows the ERFs simulated by IPSL-CM6A-LR and those estimated from the two equations from the IPCC report and revised by E16. IPSL-CM6A-LR underestimates CH_4 ERF and overestimates N_2O ERF, relative to both equations. Considering the improvements introduced by E16 to include the shortwave bands of CH_4, we use their equations (and not of
455 IPCC AR3) to recalibrate the IPSL-CM6A-LR model.
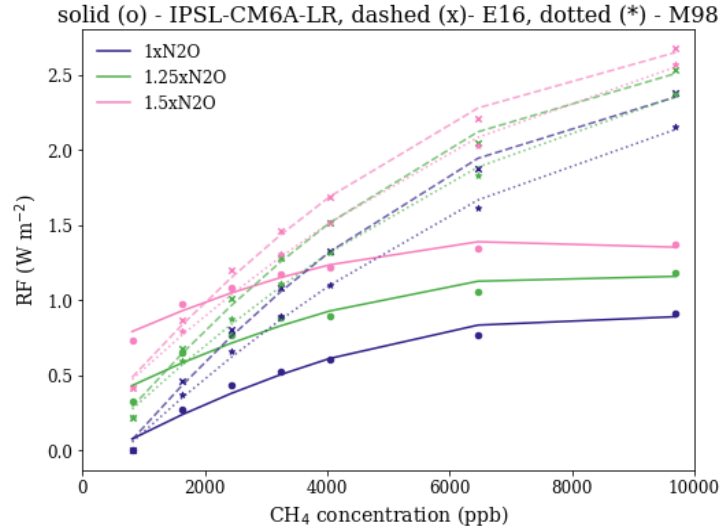
Figure A3. The ERF of CH₄ and N₂O from IPSL-CM6A-LR idealised experiments (points and fitted solid lines) and estimated from M98 (* and fitted dotted lines) and E16 (x and fitted dashed lines) equations, fitted to polynomial regressions for three levels of N₂O concentrations.

460   A system of equations can convert the input CH_4 and N_2O concentrations to the effective concentrations so that, if used in the climate model, would yield actual forcing from the equations by E16. Among several linear and nonlinear functions to relate the actual concentrations of CH_4 and N_2O with the concentrations seen by IPSL-CM6A model (effective concentrations) that have been tested, the following set of equations yielded the best fit:

$$CH_4^{effective} = CH4_{t=0} + a \times (CH4^{actual} - CH4_{t=0})^c$$
$$N2O^{effective} = N2O_{t=0} + b \times (N2O^{actual} - N2O_{t=0})^d$$

(A4)

465   The initial values of CH_4 and N_2O concentrations are fixed at the preindustrial levels ($t = 0$). Those of the effective CH_4 and N_2O concentrations are also assumed to take the same respective preindustrial levels. The Eq. (A1) is used to relate the effective concentrations of CH_4 and N_2O of IPSL-CM6A-LR to the ERF estimated by E16:

$$RF_{Etm} = RF_{CH4,\,Etm} + RF_{N2O,\,Etm}$$

$$= \left(-1.3 \times 10^{-6} \times \frac{1}{2}(CH4^{effective} + CH4_{t=0}) - 8.2 \times 10^{-6} \times \frac{1}{2}(N2O^{effective} + N2O_{t=0})\right.$$
$$\left. + 0.043\right) \times (\sqrt{CH4^{effective}} - \sqrt{CH4_{t=0}}) + (4.2 \times 10^{-6} \times \frac{1}{2}(N2O^{effective} + N2O_{t=0})$$
$$- 4.9 \times 10^{-6} \times \frac{1}{2}(CH4^{effective} + CH4_{t=0}) + 0.117) \times (\sqrt{N2O^{effective}} - \sqrt{N2O_{t=0}})$$

(A5)

470

We optimise the four parameters of Eq. (A4) by minimising the sum of squared residuals between ERF estimated by E16 equations and simulated by IPSL-CM6A-LR using a Python implementation of the Limited-memory Broyden–Fletcher–Goldfarb–Shanno bound-constrained algorithm (L-BFGS-B) that is an algorithm for solving large nonlinear optimization problems with simple bounds (Byrd et al., 1995). The cost function is defined as:

475 $\quad CF = \sum_i^{i=21}(RF_{IPSL} - RF_{Etm})^2$ $\hfill$ (A6)
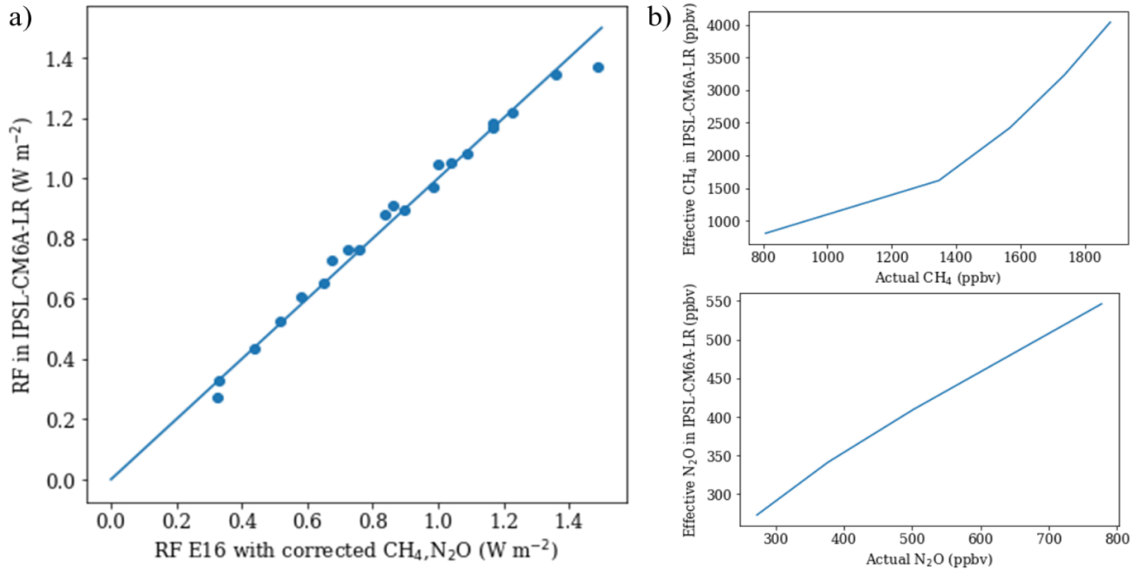
Figure A4. (a) Scatterplot of ERF simulated by IPSL-CM6A and estimated by E16 equations using the corrected effective
concentrations from Eq. (A3), and (b) The effective IPSL-CM6A-LR concentrations of CH₄ and N₂O as a function of the actual
480 **concentrations derived via a system of nonlinear functions.**

The residual error after fit equals 0.03 $(Wm^{-2})^2$ (Fig. A4). The solution of the cost function provides the estimates of four uncertain parameters for Equations 3, indicated in Table A2. The effective IPSL-CM6A-LR concentrations of CH_4 and N_2O are functions of the actual concentrations (Fig. A4b). Higher effective CH_4 and lower N_2O effective concentrations are needed for IPSL-CM6A-LR to reproduce the ERF in agreement with IPCC estimates.

485 **Table A2. Estimated parameters in Eq. (A4)**

Parameter	Estimate
a	19.44701978
b	0.84856644
c	0.49593024
d	1.13865386

The estimated parameters were applied to derive the effective IPSL-CM6A-LR concentrations for a target scenario (Fig. A5). Higher CH_4 and lower N_2O concentrations are required to reproduce the ERF correctly.
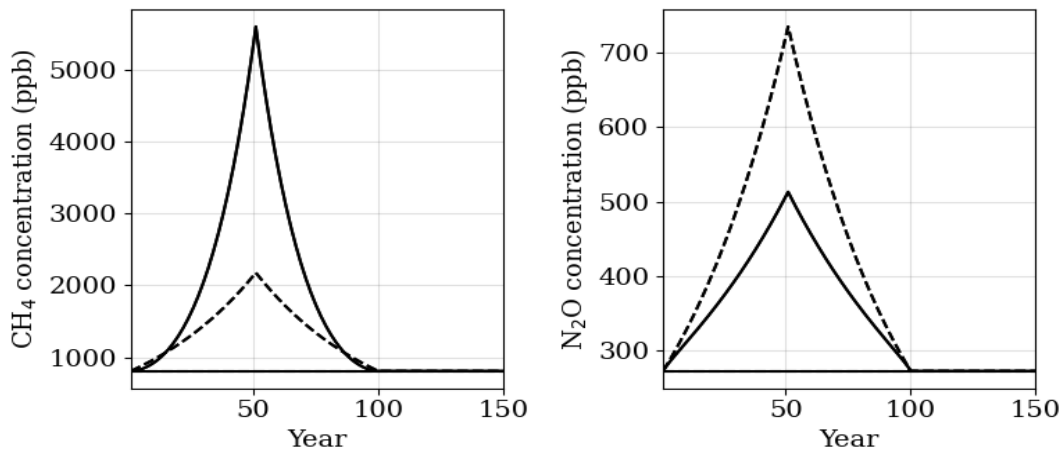
Figure A5. The actual (dashed lines) and new recalibrated effective CH₄ and N₂O IPSL-CM6A-LR concentrations (solid lines) for the CH₄-N₂O experiment of this study.

Data and materials availability

The piControl output data from the CMIP6 simulations are available from the CMIP6 archive: https://esgf-node.llnl.gov/search/cmip6 (WCRP, 2022)), additional IPSL-CM6A-LR outputs are available upon request. The Jupyter notebook and data to reproduce the figures are stored in the Zenodo archive: https://doi.org/10.5281/zenodo.12200056.

Acknowledgments

The IPSL-CM6 simulations were performed using the HPC resources of TGCC under the allocation 2022-A0120107732 and 2023-A0140107732 (project gencmip6) provided by GENCI (Grand Equipement National de Calcul Intensif). This work benefited from the technical support and discussions with Adriana Sima and Nicolas Lebas at IPSL, Arnaud Caubel and Sébastien Nguyen at LSCE (France) and Michio Kawamiya at JAMSTEC (Japan).

Funding

This work benefited from State assistance managed by the National Research Agency in France under the Programme d'Investissements d'Avenir under the reference ANR-19-MPGA-0008. We further acknowledge the Program for the Advanced Studies of Climate Change Projection (SENTAN, grant number JPMXD0722681344) from the Ministry of Education, Culture, Sports, Science and Technology, Japan and KAKENHI (JP24K20979) of the Japan Society for the Promotion of Science. We acknowledge the European Union's Horizon Europe research and innovation program under Grant Agreement N° 101056939 (RESCUE – Response of the Earth System to overshoot, Climate neUtrality and negative Emissions) and N° 101081193

(OptimESM – Optimal High Resolution Earth System Models for Exploring Future Climate Changes). P.C. acknowledges support from the CALIPSO (CArbon Losses in Plants, Soils and Ocean) project funded through the generosity of Eric and Wendy Schmidt by recommendation of the Schmidt Futures program.

510 **Author contributions**

IM and OB initiated the study. OB, Ktan and IM developed methodology and study ideas. IM and OB performed IPSL-CM6A-LR simulations. IM performed data analysis and wrote the initial draft. All authors contributed to the discussions, writing, and revising the paper.

Competing interests

515 Authors declare that they have no competing interests.

References

Abernethy, S., O'Connor, F. M., Jones, C. D., and Jackson, R. B.: Methane removal and the proportional reductions in surface temperature and ozone, Philosophical Transactions of the Royal Society A: Mathematical, Physical and Engineering Sciences, 379, 20210104, https://doi.org/10.1098/rsta.2021.0104, 2021.

520 Arora, V. K., Boer, G. J., Friedlingstein, P., Eby, M., Jones, C. D., Christian, J. R., Bonan, G., Bopp, L., Brovkin, V., Cadule, P., Hajima, T., Ilyina, T., Lindsay, K., Tjiputra, J. F., and Wu, T.: Carbon–Concentration and Carbon–Climate Feedbacks in CMIP5 Earth System Models, J. Climate, 26, 5289–5314, https://doi.org/10.1175/JCLI-D-12-00494.1, 2013.

Arora, V. K., Katavouta, A., Williams, R. G., Jones, C. D., Brovkin, V., Friedlingstein, P., Schwinger, J., Bopp, L., Boucher, O., Cadule, P., Chamberlain, M. A., Christian, J. R., Delire, C., Fisher, R. A., Hajima, T., Ilyina, T., Joetzjer, E., Kawamiya, 525 M., Koven, C. D., Krasting, J. P., Law, R. M., Lawrence, D. M., Lenton, A., Lindsay, K., Pongratz, J., Raddatz, T., Séférian, R., Tachiiri, K., Tjiputra, J. F., Wiltshire, A., Wu, T., and Ziehn, T.: Carbon–concentration and carbon–climate feedbacks in CMIP6 models and their comparison to CMIP5 models, Biogeosciences, 17, 4173–4222, https://doi.org/10.5194/bg-17-4173-2020, 2020.

Asaadi, A., Schwinger, J., Lee, H., Tjiputra, J., Arora, V., Séférian, R., Liddicoat, S., Hajima, T., Santana-Falcón, Y., and 530 Jones, C. D.: Carbon cycle feedbacks in an idealized simulation and a scenario simulation of negative emissions in CMIP6 Earth system models, Biogeosciences, 21, 411–435, https://doi.org/10.5194/bg-21-411-2024, 2024.

Bonnet, R., Swingedouw, D., Gastineau, G., Boucher, O., Deshayes, J., Hourdin, F., Mignot, J., Servonnat, J., and Sima, A.: Increased risk of near term global warming due to a recent AMOC weakening, Nature Communications, 12, 6108, https://doi.org/10.1038/s41467-021-26370-0, 2021.

535 Boucher, O. and Folberth, G. A.: New Directions: Atmospheric methane removal as a way to mitigate climate change?, Atmospheric Environment, 44, 3343–3345, https://doi.org/10.1016/j.atmosenv.2010.04.032, 2010.

Boucher, O., Halloran, P. R., Burke, E. J., Doutriaux-Boucher, M., Jones, C. D., Lowe, J., Ringer, M. A., Robertson, E., and Wu, P.: Reversibility in an Earth System model in response to CO 2 concentration changes, Environ. Res. Lett., 7, 024013, https://doi.org/10.1088/1748-9326/7/2/024013, 2012.

540 Boucher, O., Servonnat, J., Albright, A. L., Aumont, O., Balkanski, Y., Bastrikov, V., Bekki, S., Bonnet, R., Bony, S., Bopp, L., Braconnot, P., Brockmann, P., Cadule, P., Caubel, A., Cheruy, F., Codron, F., Cozic, A., Cugnet, D., D'Andrea, F., Davini, P., Lavergne, C. de, Denvil, S., Deshayes, J., Devilliers, M., Ducharne, A., Dufresne, J.-L., Dupont, E., Éthé, C., Fairhead, L., Falletti, L., Flavoni, S., Foujols, M.-A., Gardoll, S., Gastineau, G., Ghattas, J., Grandpeix, J.-Y., Guenet, B., Guez, L., E., Guilyardi, E., Guimberteau, M., Hauglustaine, D., Hourdin, F., Idelkadi, A., Joussaume, S., Kageyama, M., Khodri, M., 545 Krinner, G., Lebas, N., Levavasseur, G., Lévy, C., Li, L., Lott, F., Lurton, T., Luyssaert, S., Madec, G., Madeleine, J.-B., Maignan, F., Marchand, M., Marti, O., Mellul, L., Meurdesoif, Y., Mignot, J., Musat, I., Ottlé, C., Peylin, P., Planton, Y., Polcher, J., Rio, C., Rochetin, N., Rousset, C., Sepulchre, P., Sima, A., Swingedouw, D., Thiéblemont, R., Traore, A. K., Vancoppenolle, M., Vial, J., Vialard, J., Viovy, N., and Vuichard, N.: Presentation and Evaluation of the IPSL-CM6A-LR Climate Model, Journal of Advances in Modeling Earth Systems, 12, e2019MS002010, 550 https://doi.org/10.1029/2019MS002010, 2020.

Byrd, R. H., Lu, P., Nocedal, J., and Zhu, C.: A Limited Memory Algorithm for Bound Constrained Optimization, SIAM J. Sci. Comput., 16, 1190–1208, https://doi.org/10.1137/0916069, 1995.

Canadell, J. G., Monteiro, P. M., Costa, M. H., Da Cunha, L. C., Cox, P. M., Alexey, V., Henson, S., Ishii, M., Jaccard, S., and Koven, C.: Global carbon and other biogeochemical cycles and feedbacks., in: Climate Change 2021: The Physical Science 555 Basis. Contribution of Working Group I to the Sixth Assessment Report of the Intergovernmental Panel on Climate Change, vol. Chapter 5, Cambridge University Press, 2021.

Chimuka, V. R., Nzotungicimpaye, C.-M., and Zickfeld, K.: Quantifying land carbon cycle feedbacks under negative CO2 emissions, Biogeosciences, 20, 2283–2299, https://doi.org/10.5194/bg-20-2283-2023, 2023.

Collins, W. D., Ramaswamy, V., Schwarzkopf, M. D., Sun, Y., Portmann, R. W., Fu, Q., Casanova, S. E. B., Dufresne, J.-L., 560 Fillmore, D. W., Forster, P. M. D., Galin, V. Y., Gohar, L. K., Ingram, W. J., Kratz, D. P., Lefebvre, M.-P., Li, J., Marquet, P., Oinas, V., Tsushima, Y., Uchiyama, T., and Zhong, W. Y.: Radiative forcing by well-mixed greenhouse gases: Estimates from climate models in the Intergovernmental Panel on Climate Change (IPCC) Fourth Assessment Report (AR4), Journal of Geophysical Research: Atmospheres, 111, https://doi.org/10.1029/2005JD006713, 2006.

Etminan, M., Myhre, G., Highwood, E. J., and Shine, K. P.: Radiative forcing of carbon dioxide, methane, and nitrous oxide: 565 A significant revision of the methane radiative forcing, Geophysical Research Letters, 43, 12,614-12,623, https://doi.org/10.1002/2016GL071930, 2016.

Forster, P., Storelvmo, T., Armour, K., Collins, W., Dufresne, J.-L., Frame, D., Lunt, D. J., Mauritsen, T., Palmer, M. D., Watanabe, M., Wild, M., and Zhang, H.: The Earth's Energy Budget, Climate Feedbacks, and Climate Sensitivity, edited by: Masson-Delmotte, V., Zhai, P., Pirani, A., Connors, S. L., Péan, C., Berger, S., Caud, N., Chen, Y., Goldfarb, L., Gomis, M. 570 I., Huang, M., Leitzell, K., Lonnoy, E., Matthews, J. B. R., Maycock, T. K., Waterfield, T., Yelekçi, O., Yu, R., and Zhou, B., Climate Change 2021: The Physical Science Basis. Contribution of Working Group I to the Sixth Assessment Report of the Intergovernmental Panel on Climate Change, 923–1054, https://doi.org/10.1017/9781009157896.009, 2021.

Friedlingstein, P., Dufresne, J.-L., Cox, P. M., and Rayner, P.: How positive is the feedback between climate change and the carbon cycle?, Tellus B: Chemical and Physical Meteorology, https://doi.org/10.3402/tellusb.v55i2.16765, 2003.

575 Friedlingstein, P., Cox, P., Betts, R., Bopp, L., von Bloh, W., Brovkin, V., Cadule, P., Doney, S., Eby, M., Fung, I., Bala, G., John, J., Jones, C., Joos, F., Kato, T., Kawamiya, M., Knorr, W., Lindsay, K., Matthews, H. D., Raddatz, T., Rayner, P., Reick, C., Roeckner, E., Schnitzler, K.-G., Schnur, R., Strassmann, K., Weaver, A. J., Yoshikawa, C., and Zeng, N.: Climate–Carbon

Cycle Feedback Analysis: Results from the C4MIP Model Intercomparison, J. Climate, 19, 3337–3353, https://doi.org/10.1175/JCLI3800.1, 2006.

580 Fu, B., Gasser, T., Li, B., Tao, S., Ciais, P., Piao, S., Balkanski, Y., Li, W., Yin, T., Han, L., Li, X., Han, Y., An, J., Peng, S., and Xu, J.: Short-lived climate forcers have long-term climate impacts via the carbon–climate feedback, Nature Climate Change, 10, 851–855, https://doi.org/10.1038/s41558-020-0841-x, 2020.

Fyfe, J. C., Kharin, V. V., Santer, B. D., Cole, J. N. S., and Gillett, N. P.: Significant impact of forcing uncertainty in a large ensemble of climate model simulations, Proceedings of the National Academy of Sciences, 118, e2016549118,
585 https://doi.org/10.1073/pnas.2016549118, 2021.

Gregory, J. M., Jones, C. D., Cadule, P., and Friedlingstein, P.: Quantifying Carbon Cycle Feedbacks, J. Climate, 22, 5232–5250, https://doi.org/10.1175/2009JCLI2949.1, 2009.

Hogan, R. J. and Matricardi, M.: Evaluating and improving the treatment of gases in radiation schemes: the Correlated K-Distribution Model Intercomparison Project (CKDMIP), Geosci. Model Dev., 13, 6501–6521, https://doi.org/10.5194/gmd-
590 13-6501-2020, 2020.

Höglund-Isaksson, L., Gómez-Sanabria, A., Klimont, Z., Rafaj, P., and Schöpp, W.: Technical potentials and costs for reducing global anthropogenic methane emissions in the 2050 timeframe –results from the GAINS model, Environmental Research Communications, 2, 025004, https://doi.org/10.1088/2515-7620/ab7457, 2020.

Jackson, R. B., Abernethy, S., Canadell, J. G., Cargnello, M., Davis, S. J., Féron, S., Fuss, S., Heyer, A. J., Hong, C., and
595 Jones, C. D.: Atmospheric methane removal: a research agenda, Philosophical Transactions of the Royal Society A, 379, 20200454, 2021.

Jones, A., Haywood, J. M., and Jones, C. D.: Can reducing black carbon and methane below RCP2.6 levels keep global warming below 1.5 °C?, Atmospheric Science Letters, 19, e821, https://doi.org/10.1002/asl.821, 2018.

Jones, C. D., Ciais, P., Davis, S. J., Friedlingstein, P., Gasser, T., Peters, G. P., Rogelj, J., van Vuuren, D. P., Canadell, J. G.,
600 Cowie, A., Jackson, R. B., Jonas, M., Kriegler, E., Littleton, E., Lowe, J. A., Milne, J., Shrestha, G., Smith, P., Torvanger, A., and Wiltshire, A.: Simulating the Earth system response to negative emissions, Environmental Research Letters, 11, 095012, https://doi.org/10.1088/1748-9326/11/9/095012, 2016.

Koven, C. D., Sanderson, B. M., and Swann, A. L. S.: Much of zero emissions commitment occurs before reaching net zero emissions, Environmental Research Letters, 18, 014017, https://doi.org/10.1088/1748-9326/acab1a, 2023.

605 Lurton, T., Balkanski, Y., Bastrikov, V., Bekki, S., Bopp, L., Braconnot, P., Brockmann, P., Cadule, P., Contoux, C., Cozic, A., Cugnet, D., Dufresne, J.-L., Éthé, C., Foujols, M.-A., Ghattas, J., Hauglustaine, D., Hu, R.-M., Kageyama, M., Khodri, M., Lebas, N., Levavasseur, G., Marchand, M., Ottlé, C., Peylin, P., Sima, A., Szopa, S., Thiéblemont, R., Vuichard, N., and Boucher, O.: Implementation of the CMIP6 Forcing Data in the IPSL-CM6A-LR Model, Journal of Advances in Modeling Earth Systems, 12, e2019MS001940, https://doi.org/10.1029/2019MS001940, 2020.

610 Malley, C. S., Borgford-Parnell, N., Haeussling, S., Howard, I. C., Lefèvre, E. N., and Kuylenstierna, J. C. I.: A roadmap to achieve the global methane pledge, Environmental Research: Climate, 2, 011003, https://doi.org/10.1088/2752-5295/acb4b4, 2023.

Melnikova, I., Boucher, O., Cadule, P., Ciais, P., Gasser, T., Quilcaille, Y., Shiogama, H., Tachiiri, K., Yokohata, T., and Tanaka, K.: Carbon cycle response to temperature overshoot beyond 2 °C – an analysis of CMIP6 models, Earth's Future, 9,
615 e2020EF001967, https://doi.org/10.1029/2020EF001967, 2021.

Melnikova, I., Ciais, P., Boucher, O., and Tanaka, K.: Assessing carbon cycle projections from complex and simple models under SSP scenarios, Climatic Change, 176, 168, https://doi.org/10.1007/s10584-023-03639-5, 2023.

Mengis, N. and Matthews, H. D.: Non-CO2 forcing changes will likely decrease the remaining carbon budget for 1.5 °C, npj Climate and Atmospheric Science, 3, 19, https://doi.org/10.1038/s41612-020-0123-3, 2020.

620   Montzka, S. A., Dlugokencky, E. J., and Butler, J. H.: Non-CO2 greenhouse gases and climate change, Nature, 476, 43–50, https://doi.org/10.1038/nature10322, 2011.

Mundra, I. and Lockley, A.: Emergent methane mitigation and removal approaches: A review, Atmospheric Environment: X, 100223, https://doi.org/10.1016/j.aeaoa.2023.100223, 2023.

Myhre, G., Highwood, E. J., Shine, K. P., and Stordal, F.: New estimates of radiative forcing due to well mixed greenhouse 625   gases, Geophysical Research Letters, 25, 2715–2718, https://doi.org/10.1029/98GL01908, 1998.

Myhre, G., Shindell, D., Bréon, F. M., Collins, W., Fuglestvedt, J., Huang, J., Koch, D., Lamarque, J. F., Lee, D., and Mendoza, B.: Anthropogenic and natural radiative forcing, in: Climate change 2013: the physical science basis. Contribution of Working Group I to the Fifth Assessment Report of the Intergovernmental Panel on Climate Change, vol. Chapter 8, Cambridge University Press Cambridge, 2013.

630   Myhre, G., Forster, P. M., Samset, B. H., Hodnebrog, Ø., Sillmann, J., Aalbergsjø, S. G., Andrews, T., Boucher, O., Faluvegi, G., Fläschner, D., Iversen, T., Kasoar, M., Kharin, V., Kirkevåg, A., Lamarque, J.-F., Olivié, D., Richardson, T. B., Shindell, D., Shine, K. P., Stjern, C. W., Takemura, T., Voulgarakis, A., and Zwiers, F.: PDRMIP: A Precipitation Driver and Response Model Intercomparison Project—Protocol and Preliminary Results, Bulletin of the American Meteorological Society, 98, 1185–1198, https://doi.org/10.1175/BAMS-D-16-0019.1, 2017.

635   Nakazawa, T.: Current understanding of the global cycling of carbon dioxide, methane, and nitrous oxide, Proceedings of the Japan Academy, Series B, 96, 394–419, https://doi.org/10.2183/pjab.96.030, 2020.

Nisbet, E. G., Fisher, R. E., Lowry, D., France, J. L., Allen, G., Bakkaloglu, S., Broderick, T. J., Cain, M., Coleman, M., Fernandez, J., Forster, G., Griffiths, P. T., Iverach, C. P., Kelly, B. F. J., Manning, M. R., Nisbet-Jones, P. B. R., Pyle, J. A., Townsend-Small, A., al-Shalaan, A., Warwick, N., and Zazzeri, G.: Methane Mitigation: Methods to Reduce Emissions, on 640   the Path to the Paris Agreement, Reviews of Geophysics, 58, e2019RG000675, https://doi.org/10.1029/2019RG000675, 2020.

Nordling, K., Korhonen, H., Räisänen, J., Partanen, A.-I., Samset, B. H., and Merikanto, J.: Understanding the surface temperature response and its uncertainty to CO2, CH4, black carbon, and sulfate, Atmos. Chem. Phys., 21, 14941–14958, https://doi.org/10.5194/acp-21-14941-2021, 2021.

Nzotungicimpaye, C.-M., MacIsaac, A. J., and Zickfeld, K.: Delaying methane mitigation increases the risk of breaching the 645   2 °C warming limit, Communications Earth & Environment, 4, 250, https://doi.org/10.1038/s43247-023-00898-z, 2023.

Ou, Y., Roney, C., Alsalam, J., Calvin, K., Creason, J., Edmonds, J., Fawcett, A. A., Kyle, P., Narayan, K., O’Rourke, P., Patel, P., Ragnauth, S., Smith, S. J., and McJeon, H.: Deep mitigation of CO2 and non-CO2 greenhouse gases toward 1.5 °C and 2 °C futures, Nature Communications, 12, 6245, https://doi.org/10.1038/s41467-021-26509-z, 2021.

Palazzo Corner, S., Siegert, M., Ceppi, P., Fox-Kemper, B., Frölicher, T. L., Gallego-Sala, A., Haigh, J., Hegerl, G. C., Jones, 650   C. D., Knutti, R., Koven, C. D., MacDougall, A. H., Meinshausen, M., Nicholls, Z., Sallée, J. B., Sanderson, B. M., Séférian, R., Turetsky, M., Williams, R. G., Zaehle, S., and Rogelj, J.: The Zero Emissions Commitment and climate stabilization, Frontiers in Science, 1, https://doi.org/10.3389/fsci.2023.1170744, 2023.

Park, S.-W., Kim, J.-S., and Kug, J.-S.: The intensification of Arctic warming as a result of CO_2 physiological forcing, Nature Communications, 11, 2098, https://doi.org/10.1038/s41467-020-15924-3, 2020.

655   Pincus, R., Forster, P. M., and Stevens, B.: The Radiative Forcing Model Intercomparison Project (RFMIP): experimental protocol for CMIP6, Geosci. Model Dev., 9, 3447–3460, https://doi.org/10.5194/gmd-9-3447-2016, 2016.

Rao, S. and Riahi, K.: The Role of Non-CO_3 Greenhouse Gases in Climate Change Mitigation: Long-term Scenarios for the 21st Century, The Energy Journal, 27, 177–200, 2006.

Richardson, T. B., Forster, P. M., Smith, C. J., Maycock, A. C., Wood, T., Andrews, T., Boucher, O., Faluvegi, G., Fläschner, 660   D., Hodnebrog, Ø., Kasoar, M., Kirkevåg, A., Lamarque, J.-F., Mülmenstädt, J., Myhre, G., Olivié, D., Portmann, R. W., Samset, B. H., Shawki, D., Shindell, D., Stier, P., Takemura, T., Voulgarakis, A., and Watson-Parris, D.: Efficacy of Climate Forcings in PDRMIP Models, J Geophys Res Atmos, 124, 12824–12844, https://doi.org/10.1029/2019JD030581, 2019.

de Richter, R., Ming, T., Davies, P., Liu, W., and Caillol, S.: Removal of non-CO_2 greenhouse gases by large-scale atmospheric solar photocatalysis, Progress in Energy and Combustion Science, 60, 68–96, https://doi.org/10.1016/j.pecs.2017.01.001, 665   2017.

Schwinger, J. and Tjiputra, J.: Ocean Carbon Cycle Feedbacks Under Negative Emissions, Geophysical Research Letters, 45, 5062–5070, https://doi.org/10.1029/2018GL077790, 2018.

Schwinger, J., Tjiputra, J. F., Heinze, C., Bopp, L., Christian, J. R., Gehlen, M., Ilyina, T., Jones, C. D., Salas-Mélia, D., Segschneider, J., Séférian, R., and Totterdell, I.: Nonlinearity of Ocean Carbon Cycle Feedbacks in CMIP5 Earth System 670   Models, Journal of Climate, 27, 3869–3888, https://doi.org/10.1175/JCLI-D-13-00452.1, 2014.

Tanaka, K., Boucher, O., Ciais, P., Johansson, D. J. A., and Morfeldt, J.: Cost-effective implementation of the Paris Agreement using flexible greenhouse gas metrics, Sci Adv, 7, eabf9020, https://doi.org/10.1126/sciadv.abf9020, 2021.

Thornhill, G. D., Collins, W. J., Kramer, R. J., Olivié, D., Skeie, R. B., O'Connor, F. M., Abraham, N. L., Checa-Garcia, R., Bauer, S. E., Deushi, M., Emmons, L. K., Forster, P. M., Horowitz, L. W., Johnson, B., Keeble, J., Lamarque, J.-F., Michou, 675   M., Mills, M. J., Mulcahy, J. P., Myhre, G., Nabat, P., Naik, V., Oshima, N., Schulz, M., Smith, C. J., Takemura, T., Tilmes, S., Wu, T., Zeng, G., and Zhang, J.: Effective radiative forcing from emissions of reactive gases and aerosols – a multi-model comparison, Atmos. Chem. Phys., 21, 853–874, https://doi.org/10.5194/acp-21-853-2021, 2021.

Tokarska, K. B., Gillett, N. P., Arora, V. K., Lee, W. G., and Zickfeld, K.: The influence of non-CO_2 forcings on cumulative carbon emissions budgets, Environmental Research Letters, 13, 034039, https://doi.org/10.1088/1748-9326/aaafdd, 2018.

680   World Climate Research Programme (WCRP) Coupled Model Intercomparison Project (Phase 6): https://esgf-node.llnl.gov/search/cmip6/, last access: 6 July 2022.

Williams, R. G., Katavouta, A., and Goodwin, P.: Carbon-Cycle Feedbacks Operating in the Climate System, Current Climate Change Reports, 5, 282–295, https://doi.org/10.1007/s40641-019-00144-9, 2019.

Zhu, X., Zhuang, Q., Gao, X., Sokolov, A., and Schlosser, C. A.: Pan-Arctic land–atmospheric fluxes of methane and carbon 685   dioxide in response to climate change over the 21st century, Environmental Research Letters, 8, 045003, https://doi.org/10.1088/1748-9326/8/4/045003, 2013.

Zickfeld, K., Eby, M., Matthews, H. D., Schmittner, A., and Weaver, A. J.: Nonlinearity of Carbon Cycle Feedbacks, Journal of Climate, 24, 4255–4275, https://doi.org/10.1175/2011JCLI3898.1, 2011.

Zickfeld, K., MacDougall, A. H., and Matthews, H. D.: On the proportionality between global temperature change and cumulative CO_2 emissions during periods of net negative CO_2 emissions, Environ. Res. Lett., 11, 055006, https://doi.org/10.1088/1748-9326/11/5/055006, 2016.